

Immediate myeloid depot for SARS-CoV-2 in the human lung

Mélia Magnen^{1,*}, Ran You^{2,*}, Arjun A. Rao^{2,3}, Ryan T. Davis², Lauren Rodriguez^{3,4}, Camille R. Simoneau^{1,5}, Lisiena Hysenaj⁶, Kenneth H. Hu², The UCSF COMET Consortium⁷, Christina Love^{1,8}, Prescott G. Woodruff¹, David J. Erle¹, Carolyn M. Hendrickson¹, Carolyn S. Calfee¹, Michael A. Matthay¹, Jeroen P. Roose⁶, Anita Sil⁴, Melanie Ott^{1,5,8}, Charles R. Langelier^{1,8}, Matthew F. Krummel^{2,†}, Mark R. Looney^{1,†}

¹ Department of Medicine, University of California, San Francisco, San Francisco, CA 94143, USA

² Department of Pathology, University of California, San Francisco, San Francisco, CA 94143, USA

³ CoLabs Initiative, University of California, San Francisco, San Francisco, CA 94143, USA

⁴ Department of Microbiology and Immunology, University of California, San Francisco, San Francisco, CA 94143, USA

⁵ Gladstone Institutes, San Francisco, CA 94158, USA

⁶ Department of Anatomy, University of California, San Francisco, San Francisco, CA 94143, USA

⁷ A list of authors appears at the end of the paper.

⁸ Chan Zuckerberg Biohub, San Francisco, CA 94158, USA

* Contributed equally

† Contributed equally

Corresponding authors: matthew.krummel@ucsf.edu and mark.looney@ucsf.edu

513 Parnassus Avenue

San Francisco, CA 94143

Tel: (415) 476-9190

Abstract

In the severe acute respiratory syndrome coronavirus 2 (SARS-CoV-2) pandemic, considerable focus has been placed on a model of viral entry into host epithelial populations, with a separate focus upon the responding immune system dysfunction that exacerbates or causes disease. We developed a precision-cut lung slice model to investigate very early host-viral pathogenesis and found that SARS-CoV-2 had a rapid and specific tropism for myeloid populations in the human lung. Infection of alveolar macrophages was partially dependent upon their expression of ACE2 and the infections were productive for amplifying virus, both findings which were in contrast with their neutralization of another pandemic virus, Influenza A virus (IAV). Compared to IAV, SARS-CoV-2 was extremely poor at inducing interferon-stimulated genes in infected myeloid cells, providing a window of opportunity for modest titers to amplify within these cells. Endotracheal aspirate samples from humans with COVID-19 confirmed the lung slice findings, revealing a persistent myeloid depot. In the early phase of SARS-CoV-2 infection, myeloid cells may provide a safe harbor for the virus with minimal immune stimulatory cues being generated, resulting in effective viral colonization and quenching of the immune system.

The SARS-CoV-2 pandemic has led to over 6 million deaths worldwide. Respiratory viruses like SARS-CoV-2 are known to infect and replicate in airway epithelial cells, inducing lung injury with often fatal outcomes¹. The access to large numbers of human samples has given the opportunity to extensively study immune responses to COVID-19²⁻⁴. Unfortunately, once patients are hospitalized, the host-pathogen responses have been in progress for days or weeks, creating a challenging problem for understanding the very early host responses to SARS-CoV-2 infection in humans. While animal models are useful in this regard, they do not fully recapitulate human complexity, including appropriate expression of relevant ligands. Here, we used precision-cut lung slices (PCLS) obtained from human lungs to study early host-pathogen responses in a system replete with the full repertoire of lung stromal and immune cells.

We have previously developed a model of PCLS in the mouse lung^{5,6} that we have now applied to human lungs donated for research (Supplementary Table 1). A lung lobe was inflated using 2% low melting point agarose and 300 μm PCLSs were produced for tissue culture and direct infection with SARS-CoV-2 (USA-WA1/2020; MOI 0.1 – 1) for up to 72 hours (Fig. 1a). Imaging of the infected PCLS (Fig. 1b-c; non-infected in Extended Data Fig. 1) revealed spike staining in epithelial cells (EpCAM⁺) that were also ACE2 positive (Fig. 1b). PCLSs were also enzymatically digested for multicolor flow cytometry analysis (Fig. 1a). To further investigate infection, cells were stained for dsRNA as well as spike (Fig. 1d-e). Epithelial cells (CD45⁻ EpCAM⁺ CD31⁻) displayed both dsRNA and spike signal after 72h of SARS-CoV-2 infection (Fig. 1d and Extended Data Fig. 2a). At 72h post-infection, 4 to 10% of epithelial cells were spike⁺ and 2 to 6% dsRNA⁺. Both imaging and flow cytometry showed that SARS-CoV-2 was able to induce epithelial infection in a small-scale human lung model.

Using both imaging and flow cytometry, we also observed spike and dsRNA signal in lung immune cells (Fig. 1c and e), the former prevalent from the earliest 48-hour timepoint. Spike was colocalized to CD45⁺ ACE2⁺ cells (Fig. 1c; non-infected in Extended Data Fig. 1b) and

similarly dsRNA was found in these cells (Extended Data Fig. 2b), supporting that concept that immune cells may either be infected by SARS-CoV-2 or phagocytose the virus. Flow cytometry allowed us to further characterize spike⁺ and dsRNA⁺ immune cells (Fig. 1e). We observed significant dsRNA and spike signal in lung myeloid cells (CD45⁺ CD3⁻ CD19⁻ HLA-DR⁺ CD14⁺ cells, including interstitial macrophages, monocytes and monocyte-derived dendritic cells⁷) at 48-72h post-infection. These data support that immune cells, particularly myeloid cells, have profound and early interactions with SARS-CoV-2, potentially leading to a major role in shaping the immune response.

To further characterize the transcriptional influence of SARS-CoV-2 infection upon specific cell populations, during the first days of exposure, we applied single-cell RNA sequencing (scRNA-seq) analysis to cells obtained at various timepoints after PCLS infection (Fig. 2). Hierarchical analysis identified clusters representing highly heterogeneous lung complexity, including eight populations of non-immune cells, lymphocytes (T cells, B cells, NK), and four populations of myeloid cells (Fig. 2a and Extended Data Fig. 3a)⁸. To appreciate unique changes in lung composition and gene expression induced by SARS-CoV-2, we compared lung slices infected by either SARS-CoV-2 or Influenza A virus (IAV) (Fig. 2b). In response to IAV, the most profound change was a reduction in lung fibroblast and epithelial cell proportions, consistent with previous reports⁹. SARS-CoV-2, in contrast, produced no significant trends in lung non-immune cell populations, compared to controls. IAV was similarly destructive in the immune populations, producing a notable overall decrease in cells clustered in “Myeloid 1” (Extended Data Fig. 3a). Conversely, SARS-CoV-2 infection actually increased the myeloid fraction over time, increasing by almost 50% relative to controls at 72h (Fig. 2b).

Aligning the scRNA-seq data on the two viral genomes revealed that the main targets for IAV infection were epithelial cells and fibroblasts (Fig. 2c), consistent with the observed loss of these populations in PCLSs (Fig. 2b). In addition, IAV reads were also sporadically distributed in several other populations including immune cells. This may be attributable to the IAV entry

receptor (sialic acid) being widely distributed on the surfaces of many cell types or perhaps to phagocytosis. SARS-CoV-2 reads by comparison were distinctly enriched in myeloid cells, even at the earliest 24h timepoint. Only a few reads were identified in non-immune cells (Fig. 2c). To identify the subpopulation of myeloid cells targeted by SARS-CoV-2, the four myeloid clusters from Fig. 2a were combined and re-clustered, resulting in the definition of ten myeloid populations that included neutrophils, dendritic cells (DCs) and multiple subpopulations of monocytes and macrophages (Fig. 2d and Extended Data Fig. 3b). IAV reads remained sporadic across all 10 clusters (Fig. 2e). Conversely, SARS-CoV-2 tropism among these clusters was more selective with alveolar macrophages (AMs), IGSF21+ DCs, and monocytes accounting for the majority of significant viral reads (Fig. 2e). To account for the variable frequency of each population in Fig. 2e, we analyzed the SARS-CoV-2 read frequency and plotted this over time. This demonstrated that viral reads rose in unison in both myeloid and epithelial cell populations from 24 to 48h and then decreased in the myeloid populations at 72h (Fig. 2f). This could be the result of resolution of the infection in the PCLS, or an exhaustion of host cells targeted by the virus.

To investigate how SARS-CoV-2 affects human lung myeloid cells, we focused on the dominant AMs, which are also anatomically within the airspaces and so directly exposed to virus. A bronchoalveolar lavage (BAL) in the donor lungs (Fig. 3a) produced a sample enriched in AMs, defined here as CD45⁺ CD169⁺ HLA-DR⁺ (Extended Data Fig. 4a, d-e)¹⁰ and comprising notably few epithelial cells (<1% of live cells) (Extended Data Fig. 4b-c). AMs were analyzed for ACE2 expression (Fig. 3b), and we observed variability amongst lung donors with on average ~10-20% of ACE2⁺ AMs, but with one donor at ~80% (Fig. 3c). We incubated the cell population with SARS-CoV-2 and then analyzed cells by flow cytometry (Fig. 3a, d-e; Extended Data Fig. 4a, f-g). After 48h with SARS-CoV-2 at MOI 0.1, we detected spike in 1-10% of the AMs (Fig. 3d, Extended Data Fig. 4a). Somewhat surprisingly, an MOI of 1 did not significantly increase spike⁺ AM percentage compared to MOI 0.1 (Fig. 3d), suggesting that either cells were somehow protected at higher titers—perhaps due to increase antiviral sensing

and subsequent ISGs—or that a plateau was reached in the number of cells that were capable of being infected. At 48h, viability of AMs was high in both MOI groups, an effect that suggests the virus was not inducing AM cell death (Extended Data Fig. 4f) contrary to observations in blood monocytes from COVID-19 subjects¹¹. However, of the spike⁺ AMs, the majority were ACE2⁺ (Extended Data Fig. 4g) pointing to a specific but not obligate role for ACE2 in licensing AM viral entry. In support of this, when we used an ACE2 blocking antibody¹² incubated with AMs 2h prior to SARS-CoV-2, we always observed a significant decrease in spike⁺ AMs (Fig. 3e) but this was rarely complete, even despite using saturating concentrations of the ACE2 antibody. Taken together, these data indicate that SARS-CoV-2 entry into AMs was significantly mediated by ACE2 expression and did not require epithelial cells as an intermediate host, since our BAL preparation lacked these cells.

Macrophage infection by viruses such as IAV has long been described as abortive, but several studies have shown that the IAV H5N1 strain is capable of virus production in macrophages¹³. To study the ability of AMs that were exposed to virus to produce and release new viruses, SARS-CoV-2 and IAV (fluorescent strain, PR8-venus) were incubated with BAL cells (MOI 0.1 or 1) as above and the resulting titer in the media was then re-assessed. As a control, the same quantities of viruses were incubated only with media. After 48h of incubation, cell-free supernatant was then collected from the control (media) and BAL groups and used to infect Vero (SARS-CoV-2) or MDCK cells (IAV). After 24h, the infection of these readout cells was assessed by spike staining and flow cytometry (Fig. 3f-g, Extended Data Fig. 5a-b). By quantifying Vero cells that are positive for spike (SARS-CoV-2) or MDCK cells positive for Venus (IAV), we could quantify the infective load of virus present in cell-free supernatant after incubation with either BAL cells or cell-free media (Fig. 3a). For SARS-CoV-2, incubating the virus with BAL cells amplified virus at both MOI 0.1 and 1 compared to incubating with media alone (Fig. 3f, fold-change in Extended Data Fig. 5a). We observed the opposite effect with IAV, which decreased the amount of virus present at MOI 0.1 (Fig. 3g, fold-change in Extended Data Fig. 5b).

SARS-CoV-2 has been continuously evolving, resulting in the emergence of several variants of concern (VOC), the most pathogenic of which has been the delta variant, which we directly compared to ancestral USA-WA1/2020 in our system. As previously done, BAL cells were infected with SARS-CoV-2 viruses for 48h. To determine SARS-CoV-2 viral production by BAL cells, we used a plaque assay on BAL supernatant (Fig. 3h). BAL cells increased viral titer for both ancestral and delta (Fig. 3h, plaque assay in Extended Data Fig. 5c, fold-change in Extended Data Fig. 5d) confirming productive infection of BAL cells by these variants.

We next sorted AMs from BAL (gated as CD3⁻ CD19⁻ EpCAM⁻ CD45⁺ HLA-DR⁺ CD169⁺) before infection. After 48h infection with SARS-CoV-2 variants (Ancestral and delta) at MOI 0.1 or 1, cell-free supernatant was harvested and used for the plaque assay (Fig 3i). Consistent with results from BAL incubations, AM incubation with SARS-CoV-2 induced an increase of viral titer at both MOI 0.1 and 1 (Fig. 3j, plaque assay in Extended Data Fig. 5e, fold-change in Extended Data Fig. 5f). Anti-viral responses (ISG induction) were increased in both variants with increasing MOI most significantly with ancestral (Extended Data Fig. 5g). Taken together, our results show that incubation of AMs with SARS-CoV-2, but not IAV, leads to a productive infection of these cells and viral propagation without cell death.

To compare our findings in the isolated human lung model to clinical COVID-19 cases, endotracheal aspirates (ETA) were sampled from seven intubated COVID-19 patients (Supplementary Table S2) and analyzed by scRNA-seq (Fig. 4a). Clustering showed that the cellular population was predominantly composed of myeloid cells (Fig. 4a, far right), which contained macrophages, neutrophils, and some DCs (Fig. 4c and Extended Data Fig. 6). Analysis of SARS-CoV-2 normalized expression revealed that SARS-CoV-2 reads localized mainly to macrophages, but in some cases were also found in neutrophils and T cells (Fig. 4b), similar to prior results¹⁴. These patients were sampled at different times from 1 to 14 days after ICU admission, but the timing did not correlate with the quantity of SARS-CoV-2 reads. As in

the PCLS model, several macrophage subpopulations (phenotypes) were found to have SARS-CoV-2 reads with almost 25% of AMs being virus positive (Fig. 4d).

Finally, we analyzed differential gene expression in infected versus uninfected AMs obtained from COVID-19 ETA samples. Multiple interferon-stimulated genes (ISGs) were increased in infected compared to non-infected AMs in ETA samples (Fig. 4e), consistent with their being exposed to viruses more profoundly than neighboring cells. To ask whether ISG expression was a prominent feature of early infection, we returned to the PCLS system and compared uninfected, IAV, and SARS-CoV-2 exposure. We indeed found that AMs exposed to SARS-CoV-2 had upregulated ISGs. However, this induction was typically ~10-fold less in SARS-CoV-2, compared to IAV infection (Fig. 4f).

AMs are the sentinel immune cells in lung alveoli and relied upon to efficiently engulf and neutralize pathogens¹⁵. Here, we show that these cells are targeted by two of the most significant SARS-CoV-2 variants, leading to productive infection, viral propagation, and yet blunted interferon responses compared to IAV. These results suggest a depot effect where protective defenses are hijacked to facilitate viral production. AMs are migratory in the alveolar spaces¹⁵ and SARS-CoV-2-infected AMs could potentially spread infection to uninvolved areas of the lung leading to catastrophic viral loading of the lung, including as discussed in the accompanying manuscript, the loading of interstitial macrophage populations. We also found multiple macrophage subpopulations with SARS-CoV-2 viral reads, and it is certainly possible that these non-AM cells are also capable of productive infections. As ACE2 is an interferon-stimulated gene¹⁶, initial infection may be self-propagating, since our results indicated a critical dependency on ACE2 expression, although other viral entry mechanisms are potentially involved. As one recent example, in later stages of COVID-19 infection, and when antibodies have been generated, Fc gamma receptors appear to lead to monocyte infection¹¹. In our model, the lack of antibodies likely rules out a role of Fc receptors in viral entry into AMs. It is intriguing to consider the long-lasting effects of this macrophage depot,

which could be linked to non-resolving critical illness and long-term complications of COVID-19.

In summary, by examining the very early immune events in the human lung after SARS-CoV-2 infection, we discovered a specific tropism for lung myeloid populations and evidence of productive infection by AMs that has broad implications in unraveling the pathogenesis of severe SARS-CoV-2 infections in humans.

References

- 1 Zhou, P. *et al.* A pneumonia outbreak associated with a new coronavirus of probable bat origin. *Nature* **579**, 270-273, doi:10.1038/s41586-020-2012-7 (2020).
- 2 Combes, A. J. *et al.* Global absence and targeting of protective immune states in severe COVID-19. *Nature* **591**, 124-130, doi:10.1038/s41586-021-03234-7 (2021).
- 3 Mathew, D. *et al.* Deep immune profiling of COVID-19 patients reveals distinct immunotypes with therapeutic implications. *Science* **369**, doi:10.1126/science.abc8511 (2020).
- 4 Rodda, L. B. *et al.* Functional SARS-CoV-2-Specific Immune Memory Persists after Mild COVID-19. *Cell* **184**, 169-183 e117, doi:10.1016/j.cell.2020.11.029 (2021).
- 5 Thornton, E. E., Krummel, M. F. & Looney, M. R. Live imaging of the lung. *Curr Protoc Cytom Chapter 12*, 12 28 11-12 28 12, doi:10.1002/0471142956.cy1228s60 (2012).
- 6 Thornton, E. E. *et al.* Spatiotemporally separated antigen uptake by alveolar dendritic cells and airway presentation to T cells in the lung. *J Exp Med* **209**, 1183-1199, doi:10.1084/jem.20112667 (2012).
- 7 Baharom, F., Rankin, G., Blomberg, A. & Smed-Sorensen, A. Human Lung Mononuclear Phagocytes in Health and Disease. *Front Immunol* **8**, 499, doi:10.3389/fimmu.2017.00499 (2017).
- 8 Travaglini, K. J. *et al.* A molecular cell atlas of the human lung from single-cell RNA sequencing. *Nature* **587**, 619-625, doi:10.1038/s41586-020-2922-4 (2020).
- 9 Boyd, D. F. *et al.* Exuberant fibroblast activity compromises lung function via ADAMTS4. *Nature* **587**, 466-471, doi:10.1038/s41586-020-2877-5 (2020).
- 10 Bharat, A. *et al.* Flow Cytometry Reveals Similarities Between Lung Macrophages in Humans and Mice. *Am J Respir Cell Mol Biol* **54**, 147-149, doi:10.1165/rcmb.2015-0147LE (2016).
- 11 Junqueira, C. *et al.* FcγR-mediated SARS-CoV-2 infection of monocytes activates inflammation. *Nature*, doi:10.1038/s41586-022-04702-4 (2022).
- 12 Hoffmann, M. *et al.* SARS-CoV-2 Cell Entry Depends on ACE2 and TMPRSS2 and Is Blocked by a Clinically Proven Protease Inhibitor. *Cell* **181**, 271-280 e278, doi:10.1016/j.cell.2020.02.052 (2020).
- 13 Cline, T. D., Beck, D. & Bianchini, E. Influenza virus replication in macrophages: balancing protection and pathogenesis. *J Gen Virol* **98**, 2401-2412, doi:10.1099/jgv.0.000922 (2017).
- 14 Grant, R. A. *et al.* Circuits between infected macrophages and T cells in SARS-CoV-2 pneumonia. *Nature* **590**, 635-641, doi:10.1038/s41586-020-03148-w (2021).
- 15 Neupane, A. S. *et al.* Patrolling Alveolar Macrophages Conceal Bacteria from the Immune System to Maintain Homeostasis. *Cell* **183**, 110-125 e111, doi:10.1016/j.cell.2020.08.020 (2020).
- 16 Ziegler, C. G. K. *et al.* SARS-CoV-2 Receptor ACE2 Is an Interferon-Stimulated Gene in Human Airway Epithelial Cells and Is Detected in Specific Cell Subsets across Tissues. *Cell* **181**, 1016-1035 e1019, doi:10.1016/j.cell.2020.04.035 (2020).
- 17 Matrosovich, M., Matrosovich, T., Garten, W. & Klenk, H. D. New low-viscosity overlay medium for viral plaque assays. *Virol J* **3**, 63, doi:10.1186/1743-422X-3-63 (2006).
- 18 Brauer, R. & Chen, P. Influenza virus propagation in embryonated chicken eggs. *J Vis Exp*, doi:10.3791/52421 (2015).
- 19 McGinnis, C. S. *et al.* MULTI-seq: sample multiplexing for single-cell RNA sequencing using lipid-tagged indices. *Nat Methods* **16**, 619-626, doi:10.1038/s41592-019-0433-8 (2019).
- 20 Stuart, T. *et al.* Comprehensive Integration of Single-Cell Data. *Cell* **177**, 1888-1902 e1821, doi:10.1016/j.cell.2019.05.031 (2019).
- 21 Hafemeister, C. & Satija, R. Normalization and variance stabilization of single-cell RNA-seq data using regularized negative binomial regression. *Genome Biol* **20**, 296, doi:10.1186/s13059-019-1874-1 (2019).

- 22 Sarma, A. *et al.* Tracheal aspirate RNA sequencing identifies distinct immunological features of COVID-19 ARDS. *Nat Commun* **12**, 5152, doi:10.1038/s41467-021-25040-5 (2021).

Figure Legends

Figure 1. SARS-CoV-2 infects both epithelial and immune cells in human PCLSs. (a)

Schematic diagram of the experimental design. Human lung lobes were inflated with 2% low-melting point agarose and sectioned into 300 μm precision cut lung slices (PCLS), which were cultured in 24-well plates and infected with SARS-CoV-2 for 48 or 72h. After incubation, PCLS were either fixed and stained for confocal imaging (**b, c**) or dissociated and stained for flow cytometry (**d, e**, $n=3-4$). (**b, c**) PCLS were infected with SARS-CoV-2 for 72h at MOI 0.1 or 1 and used for confocal imaging. Alveolar spaces (Alv.) are indicated in the large image (scale bar = 50 μm). Zoom area is marked by the white rectangle. For each zoomed area, 15 or 25 μm z-stacks appears on the side with single x-y sections (Scale bar = 10 μm). (**b**) PCLS were stained for DAPI (dark blue), EpCAM (green), ACE2 (red) and spike (light blue). (**c**) PCLS were stained for DAPI (dark blue), CD45 (orange), ACE2 (red) and spike (light blue). (**d, e**) PCLS were infected at MOI 1 for 48 and 72 h. PCLS were dissociated and cell suspension was stained for flow cytometry analysis. Infection was assessed by intracellular spike and dsRNA staining in (**d**) epithelial and (**e**) myeloid cells. Grey dashed lines indicate detection limit of assays. Data indicate the mean \pm SEM. Each dot represents the average percentage of DsRNA⁺ or Spike⁺ of 2 to 3 individual lung slices from one donor. Significance was assessed using ANOVA with Sidak's multiple comparisons test. * $p<0.05$, ** $p<0.01$.

Figure 2. SARS-CoV-2 displays tropism for myeloid cells compared to IAV. (a)

A Uniform Manifold Approximation and Projection (UMAP) visualization of cells from control, SARS-CoV-2, and IAV-infected PCLS collected at distinct times. (**b**) Relative quantification of cell types from the different experimental conditions, stratified by timepoint. (**c**) Scatterplots describing the library-normalized SARS-CoV-2 expression across various cell types in SARS-CoV-2-infected PCLS (left) or IAV gene score in IAV-infected PCLS (right). (**d**) A UMAP of finely annotated myeloid cell types in the dataset. (**e**) Distribution of infected myeloid cells similar to (**c**). (**f**) The fraction (top) and numbers of SARS-CoV-2-positive cells (bottom) at different timepoints.

Figure 3. SARS-CoV-2 infection of alveolar macrophages is ACE2-dependent and amplifies viral titer. (a) Bronchoalveolar lavage (BAL) of human lungs yields cells that were plated and infected with SARS-CoV-2 at MOI 0.1 and 1 for 48h. Infected cells were analyzed by multicolor flow cytometry. Supernatant of infected BAL cells containing the virus was used to infect Vero cells. 24h after infection, infected Vero cells were quantified by flow cytometry. (b) ACE2 protein expression was assessed on AMs by flow cytometry. (c) Proportion of ACE2⁺ alveolar macrophages (AMs: CD169⁺ HLADR⁺ cells; detailed gating strategy in Extended Data Fig. 4) was measured in seven different human lungs (n=7). (d) AM infection was measured by flow cytometry using spike staining (each human lung donor response color-coded, n=7). Each dot represents the average percentage of 2 to 3 replicates from one donor. Significance was assessed using ANOVA with Dunnett's multiple comparisons test. *p<0.05. (e) ACE2 blocking antibody was added to BAL cells before infection. Cells were infected at MOI 0.1 and analyzed by flow cytometry at 48h post-infection (n=5). Each dot represents the average percentage of 2 to 3 replicates from one donor. Significance was assessed using ratio paired t-test. **p<0.01. (f) BAL cells were infected with SARS-CoV-2 for 48h at MOI 0.1 and 1 (BAL passaged). As a control, SARS-CoV-2 was incubated in cell culture media alone for 48h (Media). Cell-free supernatant was recovered and used to infect VeroE6 cells. At 24h after VeroE6 infection, cells were stained for intracellular spike expression. Using flow cytometry, infected VeroE6 percentages was determined (n=8). Each dot represents the average percentage of 2 to 3 replicates from one donor. Significance was assessed using ratio paired t-test. **p<0.01. (g) Similarly, IAV-Venus was used to infect BAL cells (MOI 0.1 and 1, BAL passaged) or incubated with media for 48h. Cell-free supernatant was used to infect MDCK cells. At 24h after MDCK infection, cells were recovered for flow cytometry. Venus expressing cells percentage was measured (n=5). Each dot represents the average percentage of 2 to 3 replicates from one donor. Significance was assessed using ratio paired t-test. ns not significant, *p<0.05. (h) Plaque assay was used as a second method to assess viral titer after SARS-CoV-2 virus (Ancestral, delta) incubation with BAL cells (n=5-6). Each dot represents the average titer of 2 replicates from one donor. Significance was assessed using ratio paired

t-test. * $p < 0.05$, ** $p < 0.01$, *** $p < 0.001$. (i) AMs were sorted from BAL samples (live, EpCAM⁻ CD45⁺ CD3⁻ CD19⁻ HLA-DR⁺ CD169⁺). (j) Following 48h of SARS-CoV-2 infection (Ancestral, delta), viral titer was determined by plaque assay in cell-free supernatant (n=5-6). Each dot represents the average titer of 2 replicates from one donor. Significance was assessed using ratio paired t-test. * $p < 0.05$.

Figure 4. Tropism of SARS-CoV-2 for myeloid cells in endotracheal aspirates from hospitalized COVID-19 subjects. (a) Endotracheal Aspirates were collected from SARS-CoV-2 infected patients and subjected to single cell RNA Seq. UMAP at far right shows landmark populations. (b) Distribution of per-cell normalized SARS-CoV-2 expression in landmark cell types. (c) UMAP projection of myeloid subtypes in endotracheal aspirates. (d) Fraction of SARS-CoV-2 positive cells per myeloid cell type (e) A volcano plot of SARS-Cov-2 positive AMs vs uninfected AMs. Interferon stimulated genes (ISGs) are highlighted in Red. (f) Log₂ Fold Change of select ISGs in the PCLS experiment in IAV- and SARS-CoV-2-infected cells at 48- and 72- hours vs control.

Extended Data Figure Legends

Extended Data Figure 1. ACE2 expression in epithelial and immune cells in non-infected

PCLS. Confocal images were obtained from non-infected controls (scale bar = 50 μm). Zoom area is marked by the white rectangles. For each zoomed area, slices appear on the side (Scale bar = 5 μm in **(a)** and 10 μm in **(b)**). **(a)** PCLS stained for EpCAM (green), ACE2 (red) and spike (light blue). **(b)** PCLS stained for CD45 (orange), ACE2 (red) and spike (light blue).

Extended Data Figure 2. SARS-CoV-2 infection drives dsRNA production in both

epithelial and immune cells in PCLS. PCLS were infected with SARS-CoV-2 and used for confocal imaging. Alveolar spaces (Alv.) are indicated in the large image (scale bar = 50 μm). Zoom area is marked by the white rectangle. For each zoomed area, z-stacks appear on the side (Scale bar = 10 μm). **(a)** PCLS stained for EpCAM (green) and dsRNA (red). **(b)** PCLS stained for CD45 (red) and dsRNA (light blue). Autofluorescence appears in green.

Extended Data Figure 3. Cell type annotations for scRNA-seq in human PCLSs. (a) A

dot plot describing the expression of the top 5 genes per identified cluster in the human PCLS dataset, used to assign cell type annotations. **(b)** A dot plot describing the expression of the top 5 genes per identified myeloid subcluster in the human PCLS dataset, used to assign myeloid cell type annotations.

Extended Data Figure 4. Human BAL cell profile and effects of SARS-CoV-2 infection.

(a) Flow cytometry gating of human BAL cells. **(b, c)** Proportions of leukocytes (CD45⁺) and epithelial cells (CD45⁻ EpCAM⁺) in total and ACE2⁺ BAL cells (n=6). **(d)** Proportion of AMs (CD45⁺ CD15⁻, CD3⁻ CD19⁻ HLA-DR⁺ CD169⁺) amongst total, live BAL cells (n=6). **(e)** PCLS were infected with SARS-CoV-2 and stained for CD45 (green), CD169 (violet) and Spike (red) before confocal imaging. Alveolar space (Alv.) is indicated in the large image (scale bar = 30 μm). Zoom areas are marked by the white rectangle (Scale bar = 15 μm). **(f)** Viability of BAL

cells infected for 48h with SARS-CoV-2 at MOI 0.1 or 1 or control (n=5). **(g)** ACE2 expression in spike⁺ AMs (n=4).

Extended Data Figure 5. Infection of BAL cells and flow-sorted AMs with SARS-CoV-2

strains. **(a)** BAL cells were infected with SARS-CoV-2 for 48h at MOI 0.1 and 1. As a control, SARS-CoV-2 was incubated in cell culture media alone for 48h. Cell-free supernatant was recovered and used to infect VeroE6 cells. At 24h after VeroE6 infection, cells were stained for intracellular spike expression. Using flow cytometry, infected VeroE6 percentages was determined (n=8). Results appear in fold change compare to media incubation. Each dot represents the average percentage of 2-3 replicates from one donor. Significance was assessed using ratio paired t-test. *p<0.05, **p<0.01. **(b)** Similarly, IAV-Venus was used to infect BAL cells (MOI 0.1 and 1) or incubated with media for 48h. Cell-free supernatant was used to infect MDCK cells. At 24h after MDCK infection, cells were recovered for flow cytometry (n=5). Venus expressing cells percentage was measured and appears as a fold change from media incubation. Each dot represents the average percentage of 2-3 replicates from one donor. Significance was assessed using ratio paired t-test. ns not significant, *p<0.05. **(c, d)** Viral titer was determined by plaque assay following 48h incubation of BAL cells and SARS-CoV-2 viruses. **(d)** Results appear as fold change from media incubated virus (n=5-6). Each dot represents the average titer of 2 replicates from one donor. Significance was assessed using ratio paired t-test. *p<0.05, **p<0.01, ***p<0.001. **(e, f)** BAL AMs (live, EpCAM⁻ CD45⁺ CD3⁻ CD19⁻ HLA-DR⁺ CD169⁺) were flow-sorted and SARS-CoV-2 strains were incubated either with AMs (MOI 0.1 – 1) or Media for 48h. Cell free supernatant was used for plaque assay in VeroE6 cells. **(f)** Results are expressed in fold change compared to media incubation (n=5-6). Each dot represents the average titer of 2 replicates from one donor. Significance was assessed using ratio paired t-test. *p<0.05. **(g)** IFITM3 staining in AMs after infection with SARS-CoV-2 (Ancestral, delta) at MOI 0.1 – 1 (n=7-9). Each dot represents the average MFI of 2-3 replicates from one donor. Significance was assessed using ANOVA with Dunnett's multiple comparisons test. ***p<0.001.

Extended Data Figure 6. Cell type annotations for scRNA-seq in human ETA samples.

A dot plot describing the expression of the top 5 genes per identified cluster in the human ETA dataset, used to assign cell type annotations.

The UCSF COMET Consortium

Cai Cathy, Jenny Zhan, Bushra Samad, Suzanna Chak, Rajani Ghale, Jeremy Giberson, Ana Gonzalez, Alejandra Jauregui, Deanna Lee, Viet Nguyen, Kimberly Yee, Yumiko Abe-Jones, Logan Pierce, Priya Prasad, Pratik Sinha, Alexander Beagle, Tasha Lea, Armond Esmalii, Austin Sigman, Gabriel M. Ortiz, Kattie Raffel, Chayse Jones, Kathleen Liu, Walter Eckalbar, Billy Huang, Norman Jones, Jeffrey Milush, Ashley Byrne, Saherai Caldera, Simon Cleary, Catherine DeVoe, Paula Hayakawa Serpa, Eran Mick, Mayra Phelps, Alexandra Tsitsiklis, K. Mark Ansel, Stephanie Christenson, Gabriela K. Fragiadakis, Arjun A. Rao, Andrew Willmore, Sidney A. Carrillo, Alyssa Ward, Kirsten N. Kangelaris, Carolyn S. Calfee, David J. Erle, Carolyn M. Hendrickson, Matthew F. Krummel, Charles R. Langelier, Prescott G. Woodruff.

Methods

Precision Cut Lung Slices (PCLS). Human donor lungs were obtained from Donor Network West. Lung lobes were inflated using 2% low-melting point agarose and incubated at 4°C^{5,6}. After agarose consolidation, 1 cm³ lung tissue was placed on the precision compresssrome VF-200 (Precisionary Instruments Inc.) for slicing. 300 µm slices were obtained and cultured in DMEM (UCSF Media Production), 1% penicillin/streptomycin (UCSF Media Production), and 10% fetal bovine serum (FBS) (Corning) in a 24-well plate.

SARS-CoV-2 infections. Vero E6 and Vero-TMPRSS2 cells (gift from Dr. Melanie Ott) were cultured in DMEM supplemented with 10% FBS, penicillin/streptomycin, and L-glutamine (Corning) in a humidified incubator at 37°C and 5% CO₂. SARS-CoV-2 virus (USA-WA1/2020 strain) was provided by Dr. Melanie Ott and propagated in Vero E6 or Vero-TMPRSS2 cells. SARS-CoV-2 B.1.617.2 (delta) variant was acquired from the California Department of Public Health, cultured in Vero-TMPRSS2 cells. For propagation, the Vero or Vero-TMPRSS2 cells were infected with the SARS-CoV-2 virus, incubated at 37°C, 5% CO₂, and at 72h the supernatant was collected. The virus was aliquoted and stored at -80°C. All work was done under Biosafety Level 3 (BSL-3) conditions. Viral titer was quantified using a plaque assay in Vero cells¹⁷. Briefly, 10-fold dilutions of the virus stock were added to Vero cells in a 12-well plate for 1 hour, after which an overlay of 1.2% Avicel RC-581 in DMEM was added. The cells were incubated at 37°C, 5% CO₂ for 96 hours. The cells were fixed with 10% formalin, stained with crystal violet, and washed with water. The plaques were counted to determine the titer of the virus stock.

Influenza A virus (IAV) infections. As a virus of reference, we used influenza A/Puerto Rico/8/34 (*PR8*, H1N1) virus labelled with Venus to infect lung slices and BAL cells. PR8-Venus IAV was a gift from Yoshihiro Kawaoka (University of Wisconsin-Madison). The virus was produced in pathogen-free fertilized chicken eggs (Charles River) as published¹⁸. In brief, eggs were kept in an egg turner for 10 days. PR8-Venus IAV was injected into the allantoic

cavity. Infected chicken embryos were incubated with the virus for 48 hours. Allantoic fluid was harvested, filtered, and snap-frozen in liquid nitrogen. Titers were determined with a hemagglutination assay. The work was done under BSL-2 conditions.

Immunofluorescence imaging. After infection, PCLS were fixed in 4% PFA for at least 30 min. After saturation in PBS with 1% BSA, slices were stained with anti-CD45 (HI30), anti-spike (40150-R007, Sino Biological), anti-dsRNA (J2) or anti-EpCAM-AF488 (9C4), for 1 hour in PBS with 1% BSA media at room temperature. PCLS were washed in PBS, counterstained with DAPI and attached to plastic coverslips using Vetbond (3M). Confocal imaging was performed using a Nikon A1R laser scanning confocal microscope with NIS-Elements software and a 16X LWD water dipping objective. Images were taken at more than 25 μm deep inside the slices to avoid the cutting artifact. 50 – 100 μm -thick images with a z-step of 1.5 μm were taken and analyzed using Imaris (Bitplane).

Flow cytometry. At selected time points, PCLS were dissociated using DNase (4 $\mu\text{g}/\text{ml}$) and Collagenase IV (200U/ml) at 37°C for 30min. Cells were filtered and stain for viability and surface markers (Supplementary Table 3). After fixation and permeabilization (BD cytofix/Cytoperm), cells were stained for spike and dsRNA (Supplementary Table 3). Data were collected using the BD LSRII Cytometer and analyzed using FlowJo version 10 (BD Biosciences).

Bronchoalveolar lavage. A bronchoalveolar lavage (BAL) was done in a human lung lobe using ice-cold PBS. BAL cells were filtered and red blood cells lysed. BAL cells were plated in 24 well plates at 5×10^5 cells per well in DMEM, 1% PS, 10% FBS containing 50 ng/ml of rhM-CSF (300-25, Peprotech). For selected experiments, BAL cells were treated for 2h before infection with an ACE2 blocking antibody at 10 $\mu\text{g}/\text{ml}$ (AF933, R&D systems). SARS-CoV-2 was added to the cells at MOI 0.1 or 1. After 48h of infection, cells were recovered and stained for viability and surface markers (Supplementary Table 4). After fixation and permeabilization,

cells were stained for intracellular spike expression. In selected experiments, AMs (live, EpCAM-, CD3-, CD19-, CD45+, HLA-DR+, CD169+) were flow-sorted prior to infection with SARS-CoV-2 using FACSAria Fusion (BD Biosciences).

Virus replication assay. BAL cells were infected for 48h either with SARS-CoV-2 or IAV-Venus at MOI 0.1 or 1. At the end of the incubation, cell-free supernatant was recovered. This solution was used as inoculum for Vero E6 cells (SARS-CoV-2) or MDCK cells (IAV-Venus). After 24 hours of incubation, cells were recovered and infection was assessed by flow cytometry.

Single-cell RNA-sequencing. PCLS were dissociated as described above and dead cells were removed using Miltenyi Dead Cell Removal Kit (130-090-101, Miltenyi Biotec). For the multiplexing purpose, cells were then labeled with lipid modified oligonucleotides (LMO) and barcode oligos using the Multi-seq technique¹⁹. Cells were counted and the targeted cell number for loading was 8000 cells per sample. 10X encapsulation and library construction were done using Chromium Next GEM Single Cell 3' Reagent Kits v3.1 per the manufacturer's instruction. Multi-seq library preparation was done as previously described¹⁹. Libraries were mixed at an approximate 10:1 molar ratio of gene expression to LMO barcodes for sequencing. The sequencing was done on the Illumina NovaSeq 6000 using 10X Genomics recommended sequencing parameters.

Data pre-processing of 10x Genomics Chromium scRNA-seq data. Sequencer-generated bcl data (Gene expression and Lipid Hashtag) was demultiplexed into individual fastq libraries using the mkfastq command on the Cellranger 3.0.2 suite of tools (<https://support.10xgenomics.com>). Feature-barcode matrices for all samples were generated using the Cellranger count command. Briefly, raw gene-expression fastqs were aligned to the GRCh38 reference genome annotated with Ensembl v85, and Lipid Hashtag fastqs were processed to count the incidences of each expected index per cell. Feature-barcode matrices

were read into Seurat 4.0.1²⁰ and poorly-captured genes (in < 3 cells) were dropped from the analyses. Matrices were further filtered to remove events with greater than 20% mitochondrial content, events with greater than 50% ribosomal content, or events with fewer than 100 total genes.

Data quality control and normalization. The gene expression count matrices were normalized, and variance stabilized using negative binomial regression using the scTransform algorithm²¹ in the Seurat package. Cellular mitochondrial content, ribosomal content, and cell cycle state were regressed out of the data at this stage to prevent any confounding signal. The normalized matrices were transformed into a lower subspace using Principal Component Analysis (PCA) and 50 PCs per samples were used to generate Uniform Manifold Approximation and Projection (UMAP) visualizations. Cell clustering via expression was conducted using the Louvain algorithm. Cluster identities were assigned using Gene scores generated via the Seurat AddModuleScore function on a list of gene sets obtained from the Human Lung Cell Atlas.

Demultiplexing of pooled single-cell libraries. In Lipid hashtagged libraries, the raw lipid tag counts were normalized using the Centered Log Ratio method (CLR) where HTO counts are divided by the geometric mean for that HTO across all cells and then log normalized. The resulting matrix was demultiplexed into donor samples using the Seurat HTODemux function²¹ using default parameters.

Data integration and batch correction. scTransformed count matrices from all samples were integrated together using the in-built integration method provided by Seurat. The following commands were run in order, to integrate datasets `SelectIntegrationFeatures` to identify shared “anchor” features for integration, `PrepSCTIntegration` to subset objects based on identified anchor features, `FindIntegrationAnchors` to identify anchor points between datasets based on the anchor features, and finally `IntegrateData` to actually integrate the datasets

based on the computed anchors. Downstream processing (PCA, UMAP, clustering and cluster assignment) was conducted similarly to the individual libraries.

Endotracheal aspirates samples (ETA). Endotracheal aspirate (ETA) samples were prospectively collected from seven adults requiring mechanical ventilation for the acute respiratory distress syndrome (ARDS) from COVID-19 as part of the COVID Multiphenotyping for Effective Therapies (COMET) study, as previously described²². Patients were enrolled at two tertiary care hospitals in San Francisco, CA (UCSF Medical Center, Zuckerberg San Francisco General Hospital) under research protocol 20-30497 approved by the University of California San Francisco Institutional Review Board. ETA samples were collected within 1-14 days of intubation for scRNA-sequencing.

Statistical analyses. Statistical analysis was performed using GraphPad Prism v7.0e. Ratio paired t-test was used to compare two paired groups. Multiple group comparisons were analyzed by one-way ANOVA with Sidak's multiple comparisons test. When comparing paired values, one-way ANOVA with Dunnett's multiple comparisons test was used.

Acknowledgements. This work was supported by NIH funding as follows: NIAID-sponsored Immunophenotyping Assessment in a COVID-19 Cohort (IMPACC) Network [NIH/NIAID U19 AI1077439], R35 HL140026 (C.S.C.), R01 AI052116 (M.F.K.), R01 AI160167 (M.R.L.), R35 HL161241 (M.R.L.), P30 DK063720 (UCSF Flow Cytometry CoLab), and Shared Instrument Grant 1S10OD021822-01 (UCSF Flow Cytometry CoLab). We also acknowledge funding from COVID-19 Fast Grants (M.O. and M.R.L.), UCSF Clinical and Translational Science Institute (CTSI), and the UCSF ImmunoX Initiative. M.O. thanks the Rodenberry foundation, Pam and Ed Taft, the Innovative Genomics Institute, and the Gladstone Institutes for their support.

Author contributions.

All authors contributed to manuscript preparation. Conceptualization: MM, RY, MFK, MRL. Experimentation: MM, RY, LR, CRS, LH. Human samples: The UCSF COMET Consortium, PGW, DJE, CMH, CSC, MAM, CRL. Data analysis: MM, RY, RTD, AAR, KHH, MFK, MRL. Reagents: AS, MO. Supervision: MFK, MRL. Manuscript writing: MM, RY, AAR, MFK, MRL.

Competing interests. The authors declare no competing interests.

Supplementary Table 1. Human lung donor demographics and experimental assignments.

Donor	Gender	Race/ Ethnicity	Age	Cause of death	Donation	Comorbidities	Smoking (>20PY)	Experiment Type
1	M	White	63	Anoxia	DBD	Hypertension, Pulmonary nodules	yes	BAL
2	F	White	49	Anoxia	DCD	Asthma, COPD, Sepsis pneumonia	yes	PCLS flow, PCLS imaging
3	F	White	37	Anoxia	DBD	None	no	PCLS flow, PCLS imaging
4	M	White	51	Stroke	DBD	Diabetes, CAD, Hypertension	no	PCLS flow, PCLS imaging
5	M	White	47	Stroke	DCD	None	no	PCLS flow, PCLS imaging
6	M	Asian/White	32	Head Trauma	DBD	Diabetes	no	PCLS flow
7	F	Hispanic	44	Stroke	DBD	None	no	PCLS flow, PCLS imaging
8	M	Asian	50	Stroke	DCD	Asthma, Hypertension	no	PCLS flow
9	M	White	46	Suicide	DCD	None	yes	PCLS flow
10	F	Asian	56	Stroke	DCD	Hypertension	no	PCLS imaging
11	F	White	57	Stroke	DBD	None	no	PCLS flow, PCLS imaging
12	M	Hispanic	27	Head Trauma	DBD	Asthma	no	PCLS SCS
13	M	White	43	Anoxia	DCD	None	no	BAL, PCLS flow, PCLS imaging
14	F	Hispanic	44	Stroke	DBD	None	no	PCLS imaging, PCLS SCS
15	M	White	43	Anoxia	DCD	None	no	PCLS flow
16	M	Hispanic	57	Stroke	DBD	None	no	BAL
17	M	White	50	Head Trauma	DCD	Hypertension	no	BAL
18	M	White	31	Head Trauma	DCD	None	no	BAL
19	M	Hispanic	50	Stroke	DBD	Hypertension	no	BAL
20	F	White	62	Head Trauma	DBD	Cancer	no	BAL
21	M	White	27	Anoxia	DBD	None	no	BAL
22	F	Hispanic	39	Head trauma	DBD	None	no	BAL
23	F	White	58	Anoxia	DCD	Diabetes, Hypertension	no	BAL
24	F	White	62	Anoxia	DCD	COPD, Hypertension, Hypersensitivity Lung Disease, and diabetes	yes	BAL
25	M	White	32	Anoxia	DCD	Asthma	no	BAL
26	M	Hispanic	25	Anoxia	DCD	None	no	BAL
27	M	Hispanic	33	Head trauma	DBD	Hypertension	no	BAL
28	M	White	33	Anoxia	DBD	Diabetes	yes	BAL
29	M	White	46	Stroke	DBD	Asthma	no	BAL

DBD: donation after brainstem death

COPD: chronic obstructive pulmonary disease

BAL: bronchoalveolar lavage

PCLS Imaging: precision cut lung slice immunofluorescence imaging

DCD: donation after cardiac death

CAD: coronary artery disease

PCLS flow: precision cut lung slice flow cytometry

SCS: single-cell RNA sequencing

Supplementary Table 2. COVID-19 endotracheal aspirate samples.

Subject	Age	Gender	Ethnicity	ARDS (Y/N) Berlin definition	ETT sampling after intubation (days)	P/F ratio at time of ETT sampling	ICU LOS (days)	Hospital LOS (days)	Death (Y/N)
1 (1)	34	F	White	Yes	0	180	12	14	No
2 (365)	55	M	Unknown	No	2	ND	35	60	No
3 (414)	58	M	Other / Multiple Races	No	1/3	165	19	27	No
4 (415)	62	F	Black / African American	No	2	124.3	14	21	No
5 (419)	68	M	Other / Multiple Races	Yes	7	175	26	50	No
6 (476)	59	M	White	No	12	ND	44	78	No
7 (389)	66	F	White	Yes	2	144	39	55	No

ARDS: acute respiratory distress syndrome

ETT: endotracheal tube

P/F ratio: PaO₂/FiO₂

ICU LOS: intensive care unit length of stay

Hospital LOS: hospital length of stay

Supplementary Table 3. Flow cytometry panel for PCLS experiments.

Staining	Antibody (clone)	Lot number	Dye	Catalog number (Supplier)
Surface Staining	CD169	1621398	AF594	FAB5197T (R&D Systems)
	ACE2	BJ07067522	PE	bs-1004R (BIOSS)
	EpCAM	B250368	BV650	324226 (BioLegend)
	CD31 (WM59)	8232937	BV605	562855 (BD Biosciences)
	CD45 (HI30)	B333796	BV421	304032 (BioLegend)
	CD14 (M5E2)	B275828	BV711	301838 (BioLegend)
	CD3 (SK7)	0314461	BB700	566575 (BD Biosciences)
	CD19 (SJ25C1)	1069967	BB700	566396 (BD Biosciences)
	Zombie (viability)	B331984	NIR	77184 (BioLegend)
HLA-DR (G46-6)	1266420	BUV395	564040 (BD Biosciences)	
Intracellular Staining	Spike	1619059	AF647	FAB105805R (R&D Systems)
	dsRNA (J2)	J2-2007	AF488	10010 (Scicons)

Supplementary Table 4. Flow cytometry panel for BAL experiments.

Staining	Antibody	Lot number	Dye	Reference
Surface Staining	CD169	1621398	AF594	FAB5197T (R&D Systems)
	ACE2	BJ07067522	PE	bs-1004R (BIOSS)
	CD15 (W6D3)	1089776	BV786	741013 (BD Biosciences)
	CD16 (3G8)	B321940	BV605	302040 (BioLegend)
	CD45 (HI30)	B333796	BV421	304032 (BioLegend)
	CD14 (M5E2)	B275828	BV711	301838 (BioLegend)
	CD3 (SK7)	0314461	BB700	566575 (BD Biosciences)
	CD19 (SJ25C1)	1069967	BB700	566396 (BD Biosciences)
	Zombie (viability)	B331984	NIR	77184 (BioLegend)
	HLA-DR (G46-6)	1266420	BUV395	564040 (BD Biosciences)
Intracellular Staining	Spike	1619059	AF647	FAB105805R (R&D Systems)
	IFITM3 (EPR5242)	GR3416716-1	AF488	Ab198559 (Abcam)

Figure 1

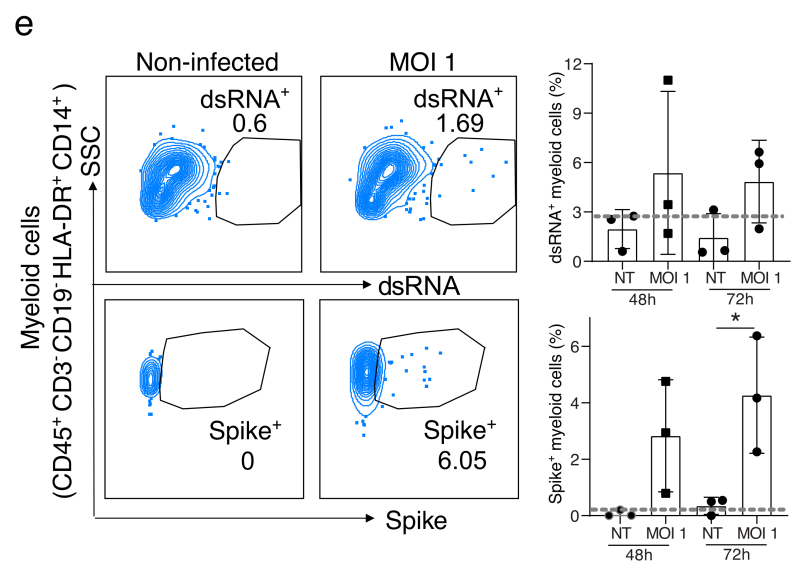
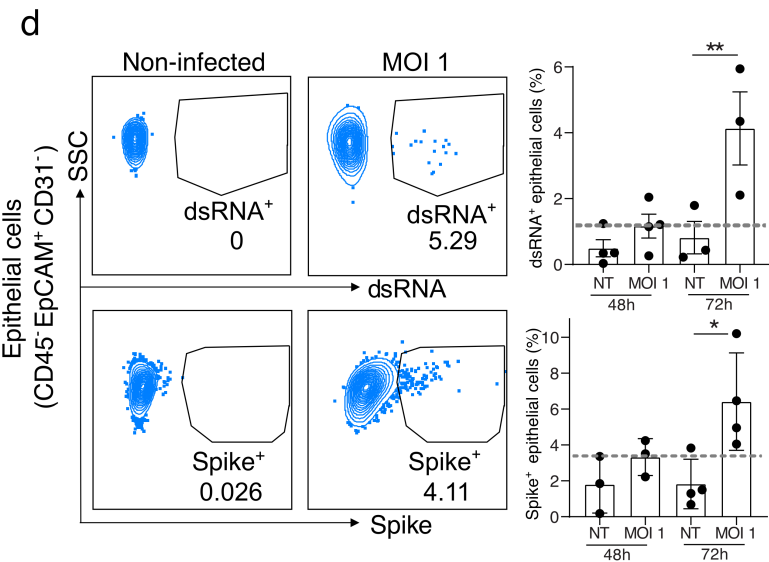
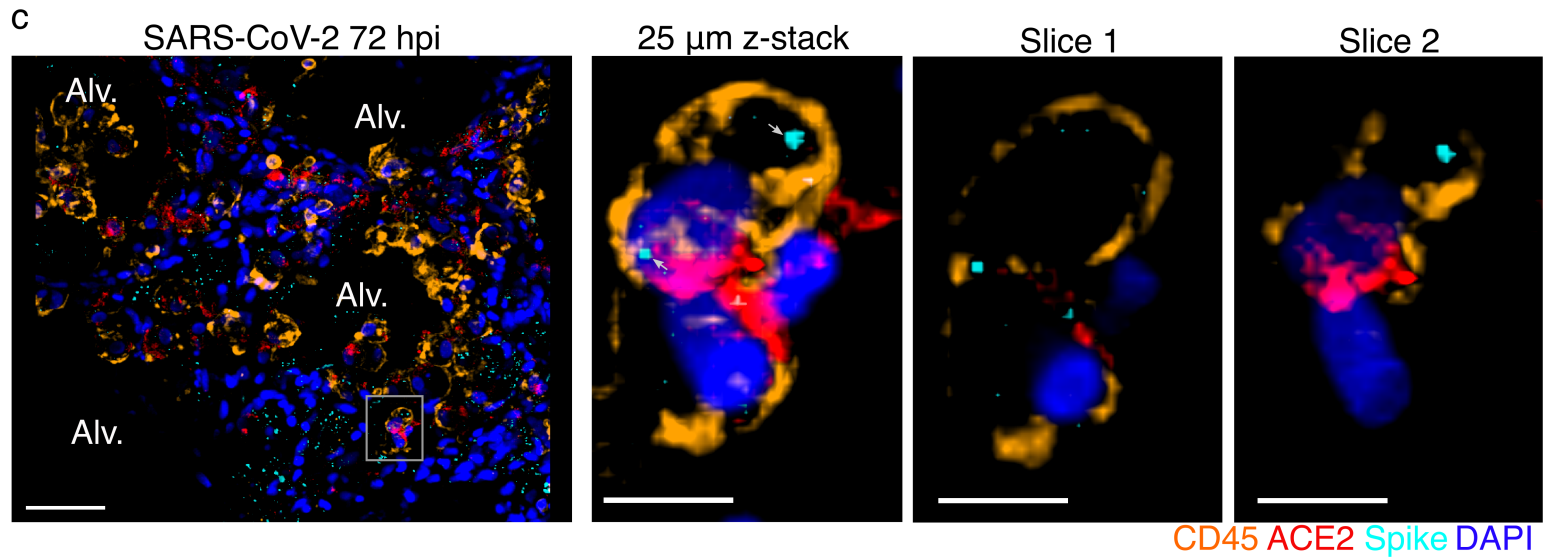
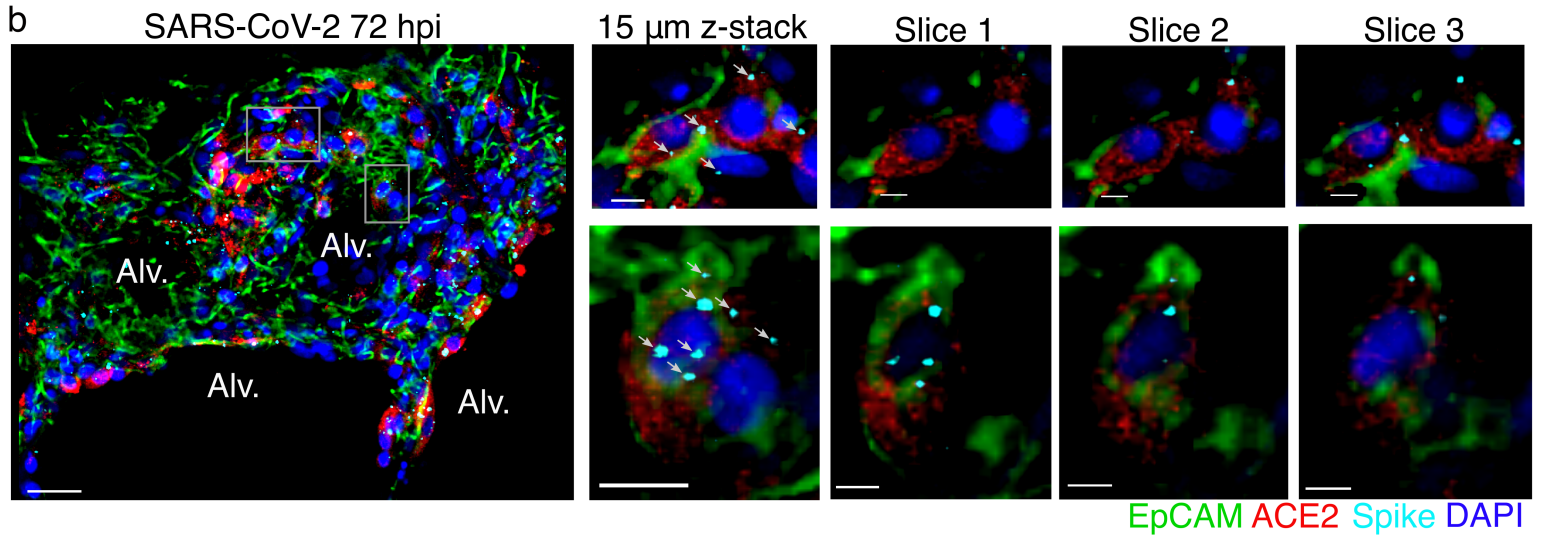
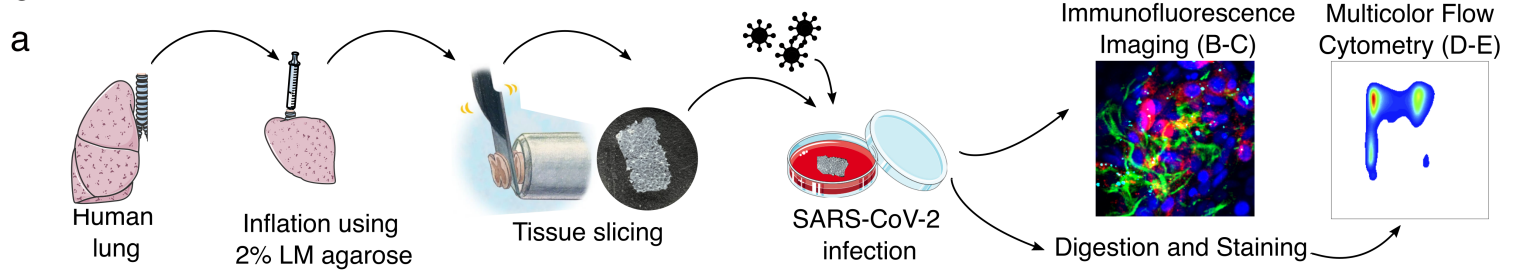


Figure 2

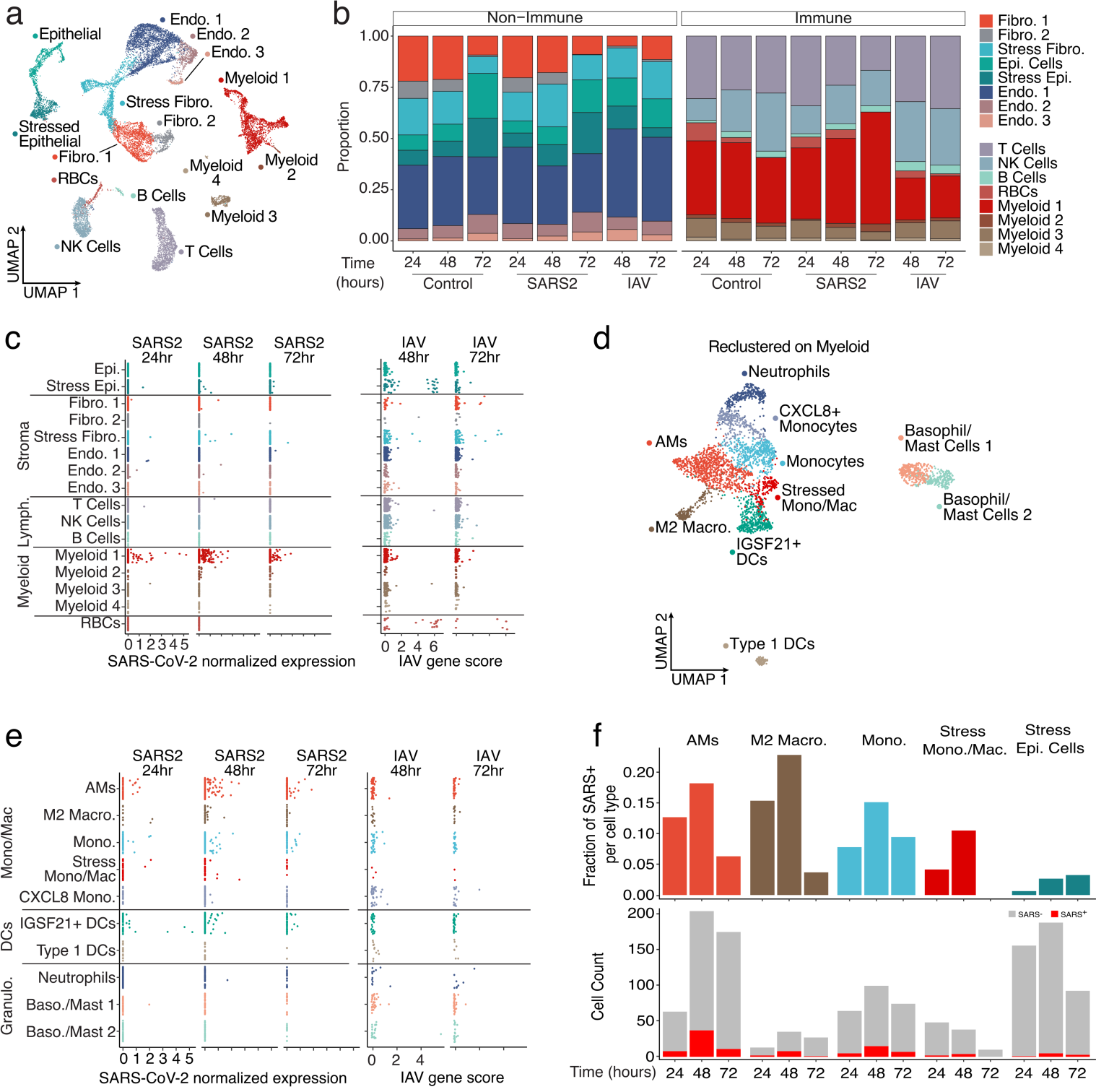


Figure 3

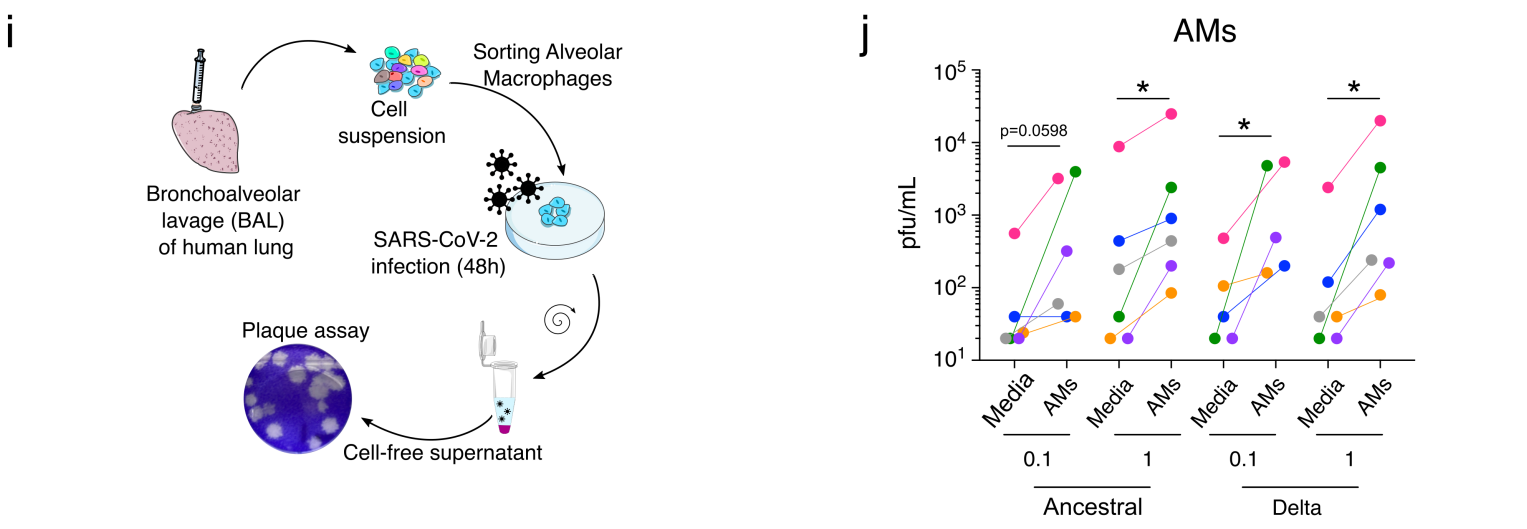
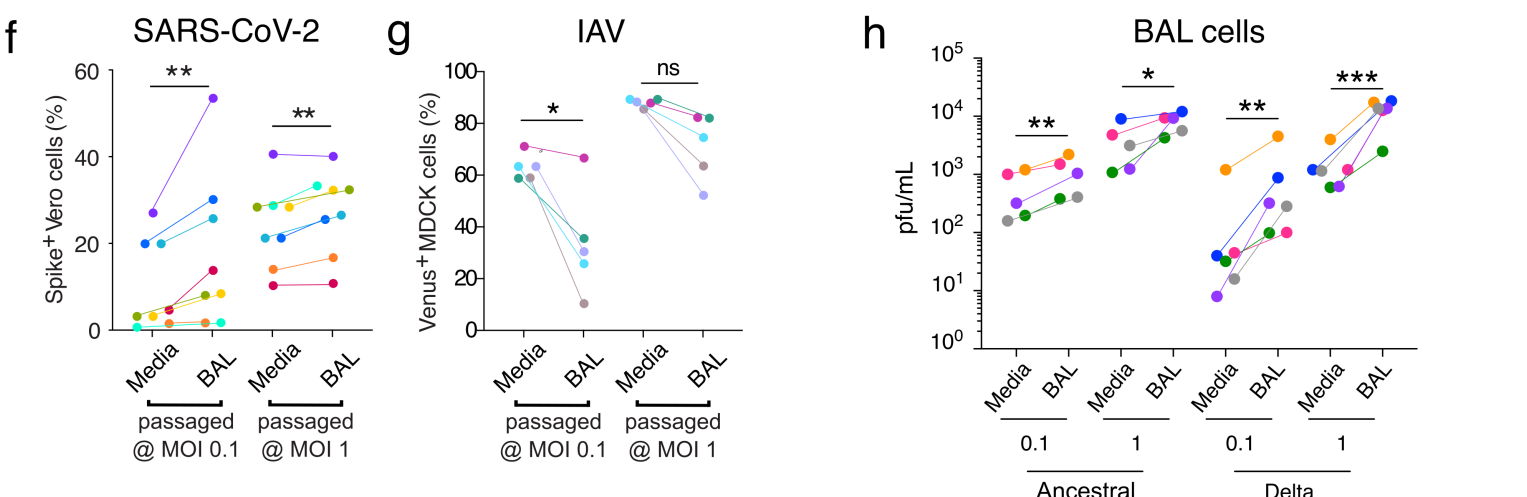
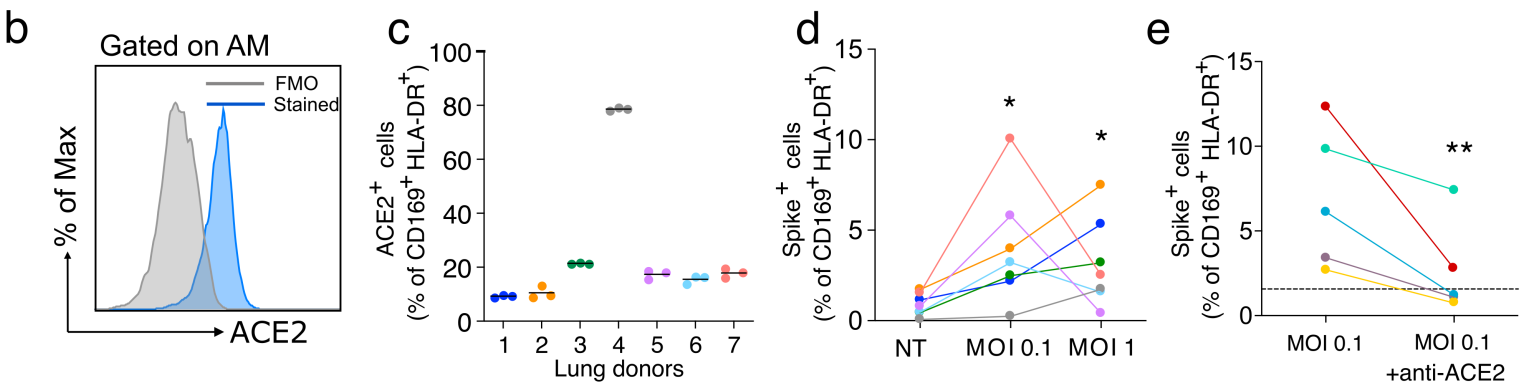
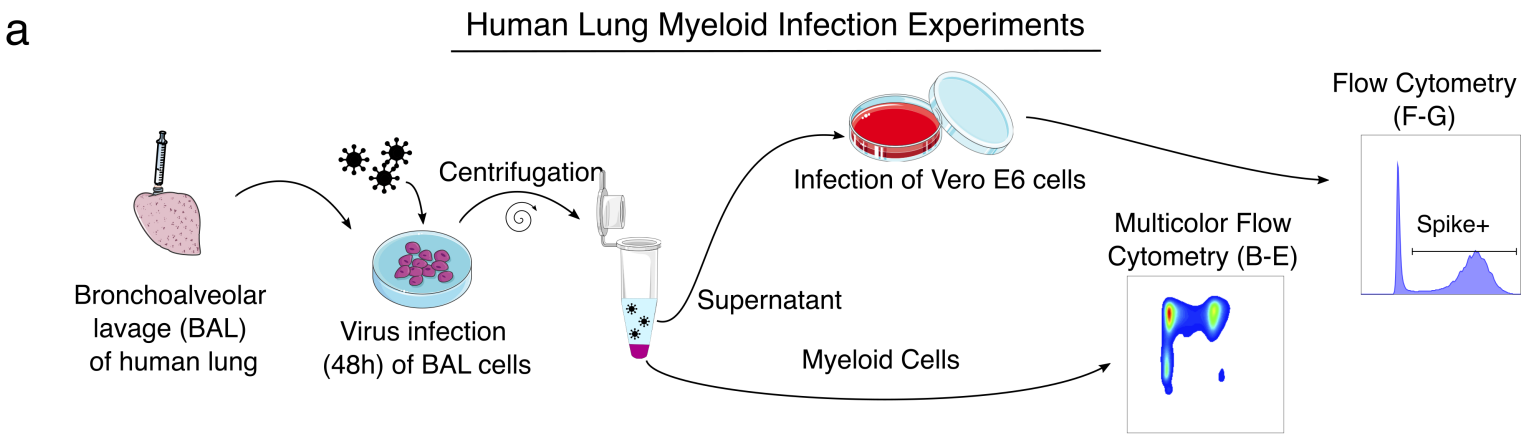
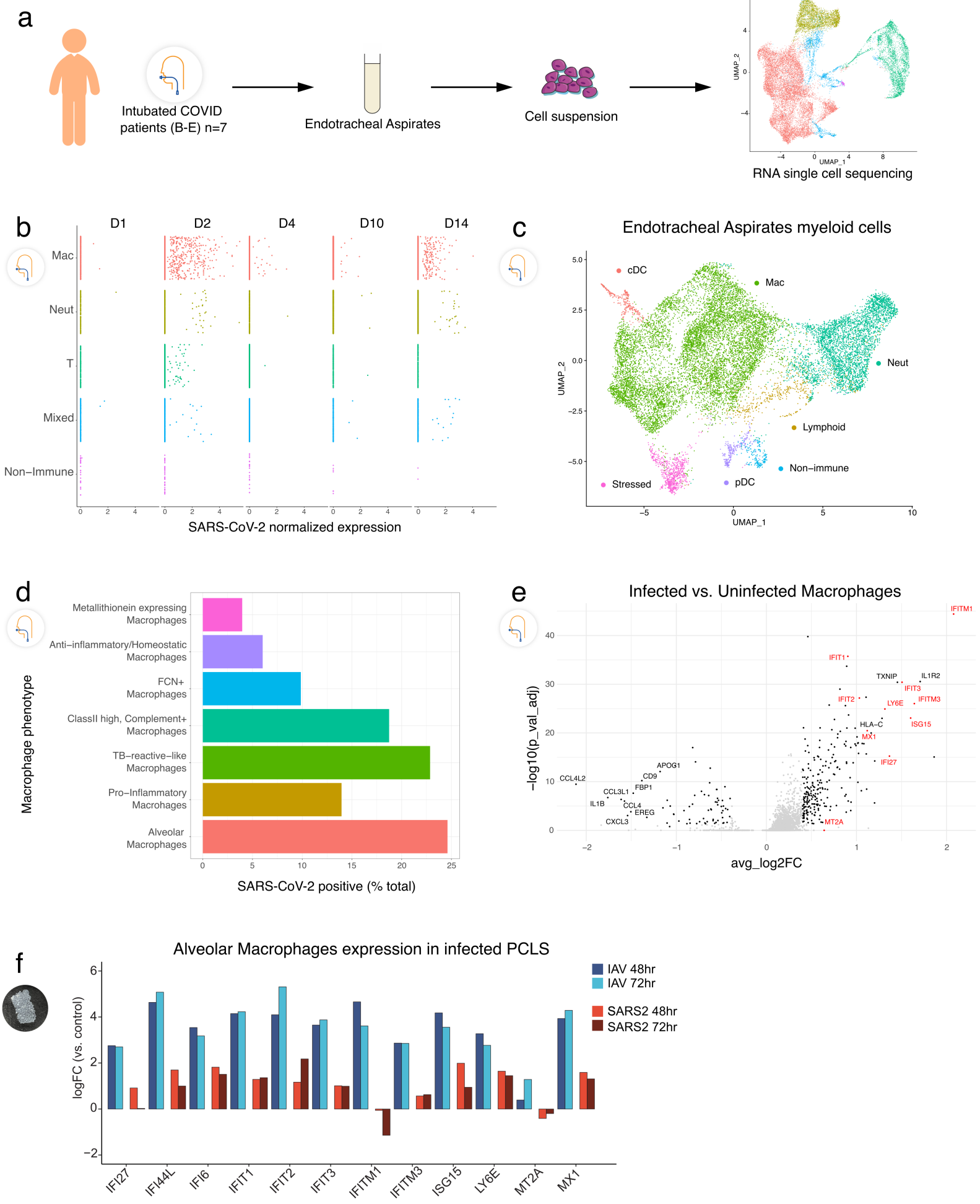
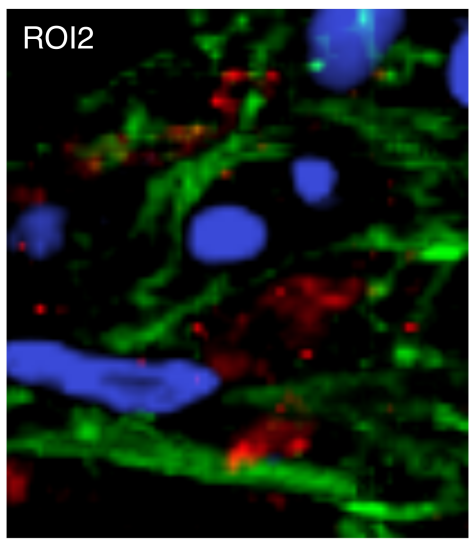
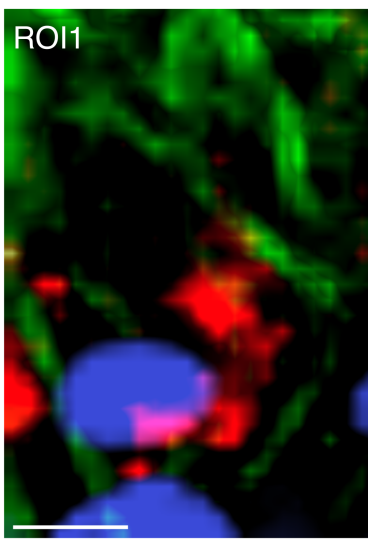
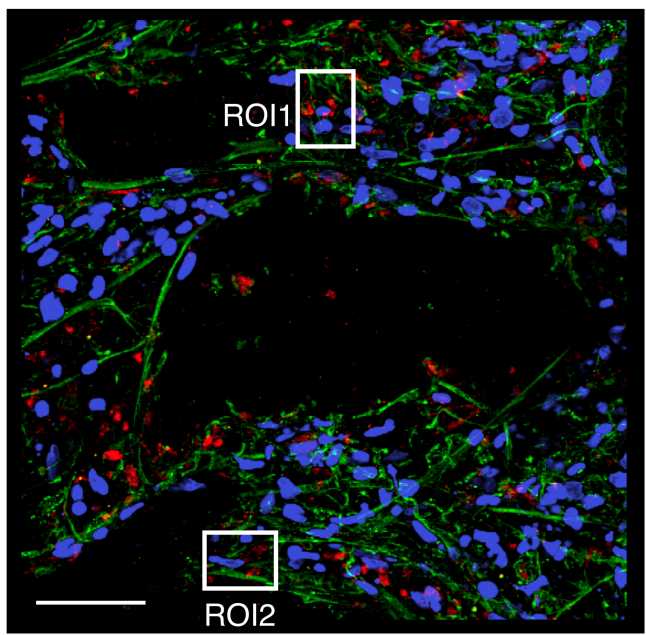


Figure 4



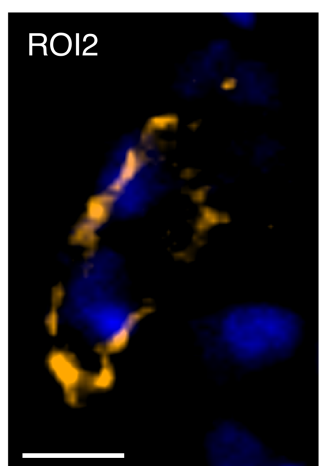
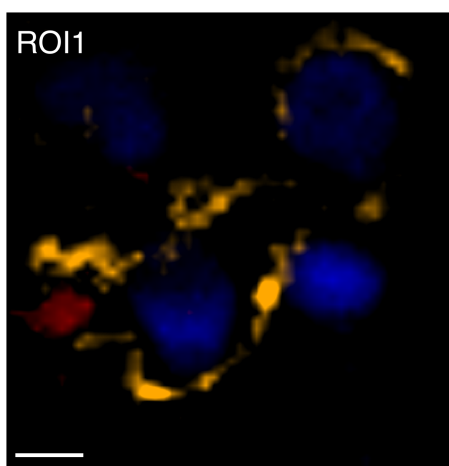
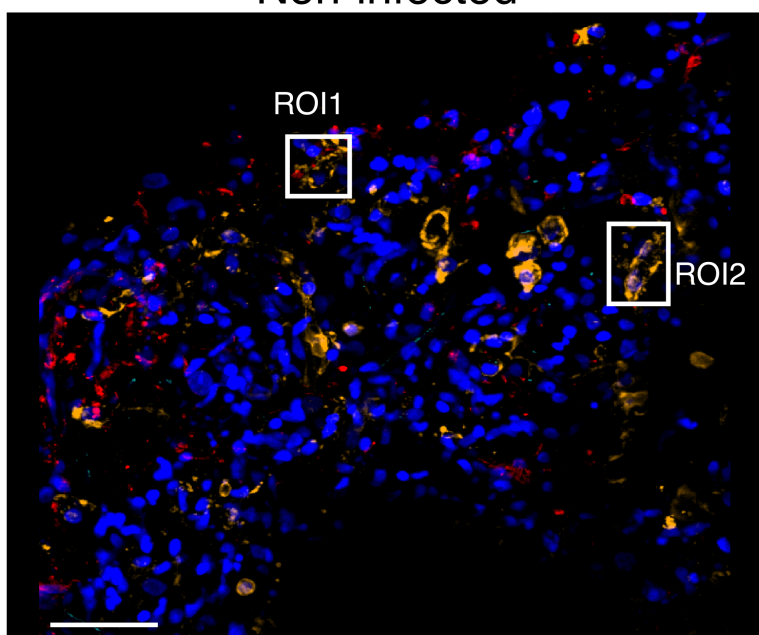
Extended Data Figure 1

a Non-infected



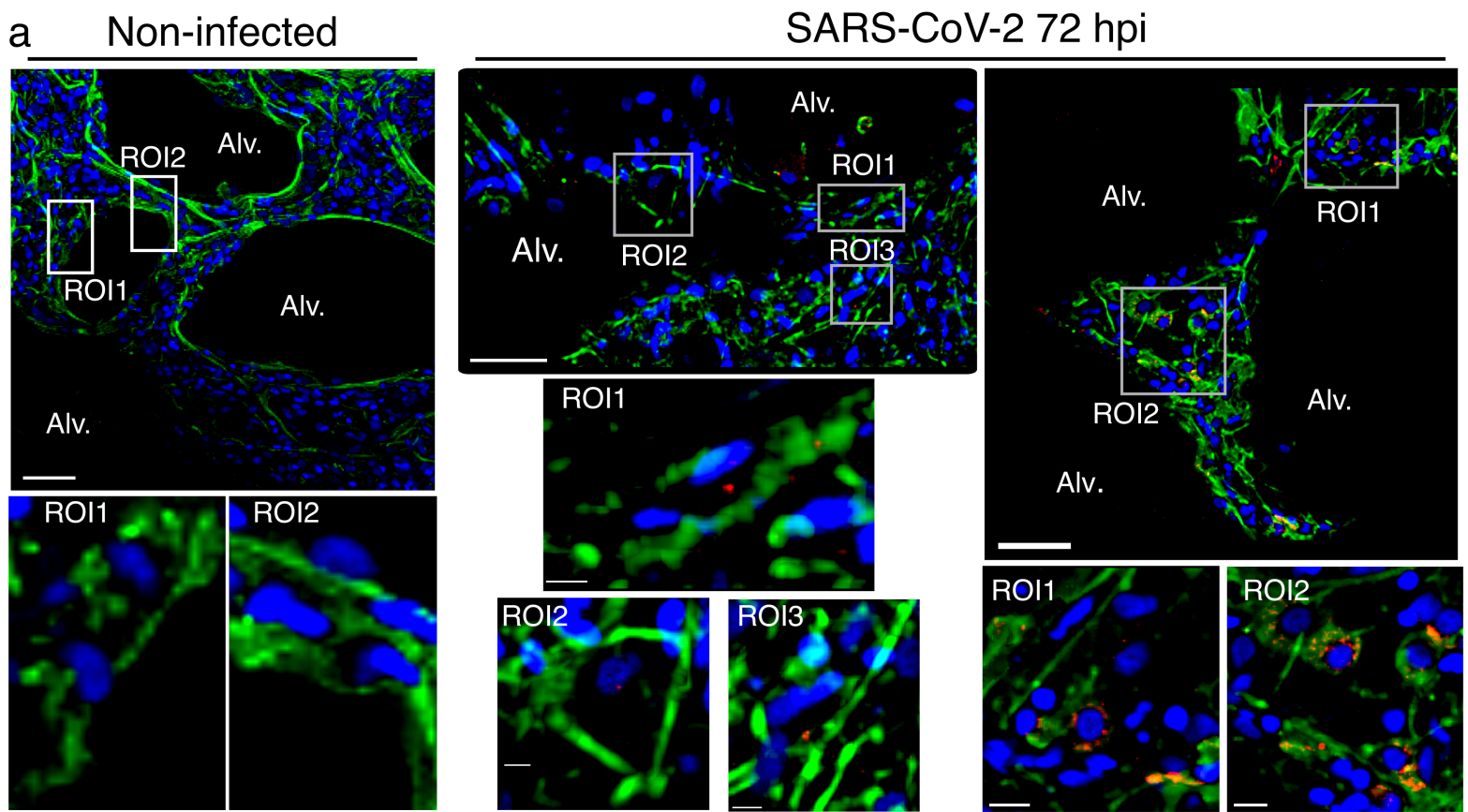
EpCAM ACE2 Spike DAPI

b Non-infected

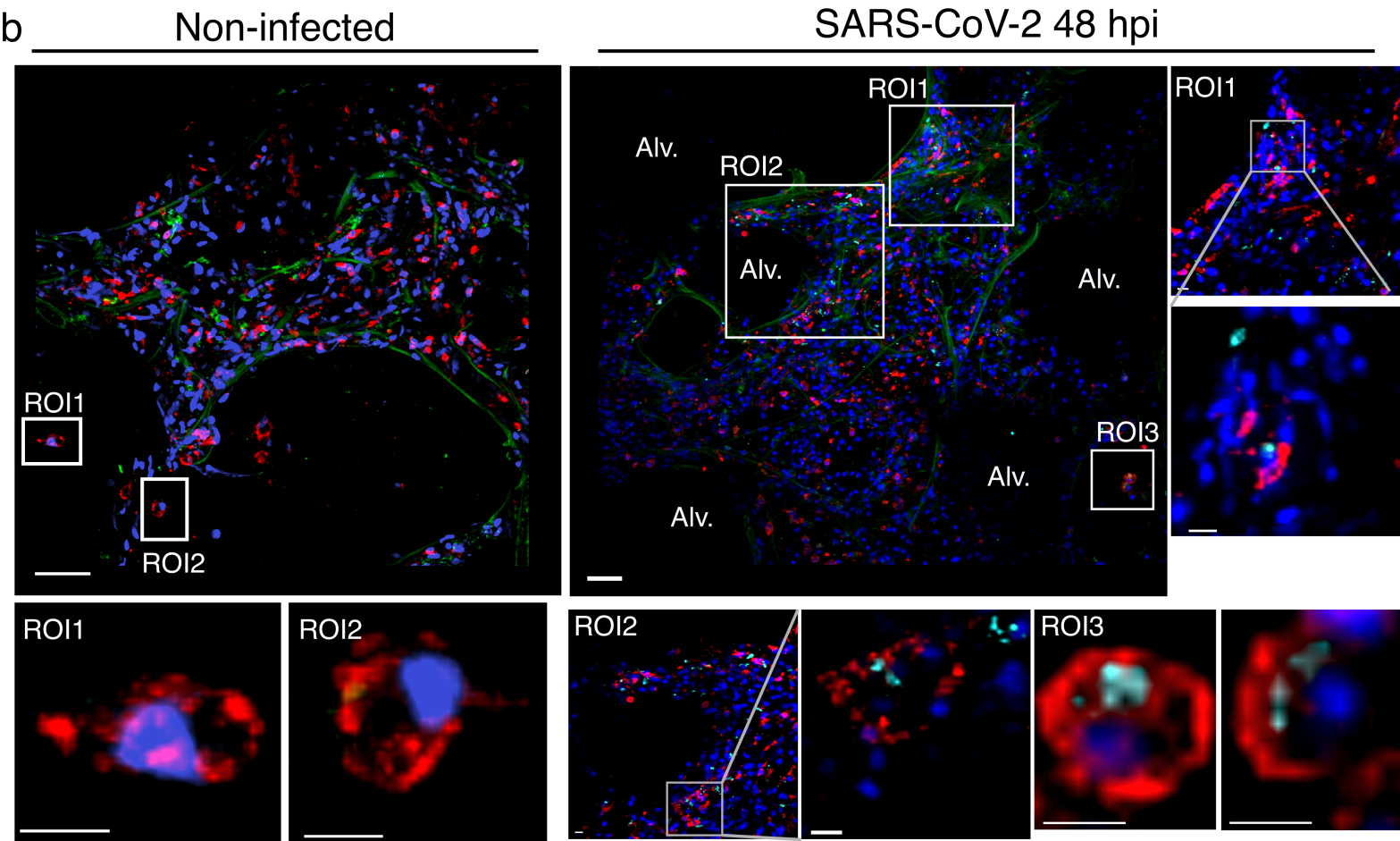


CD45 ACE2 Spike DAPI

Extended Data Figure 2

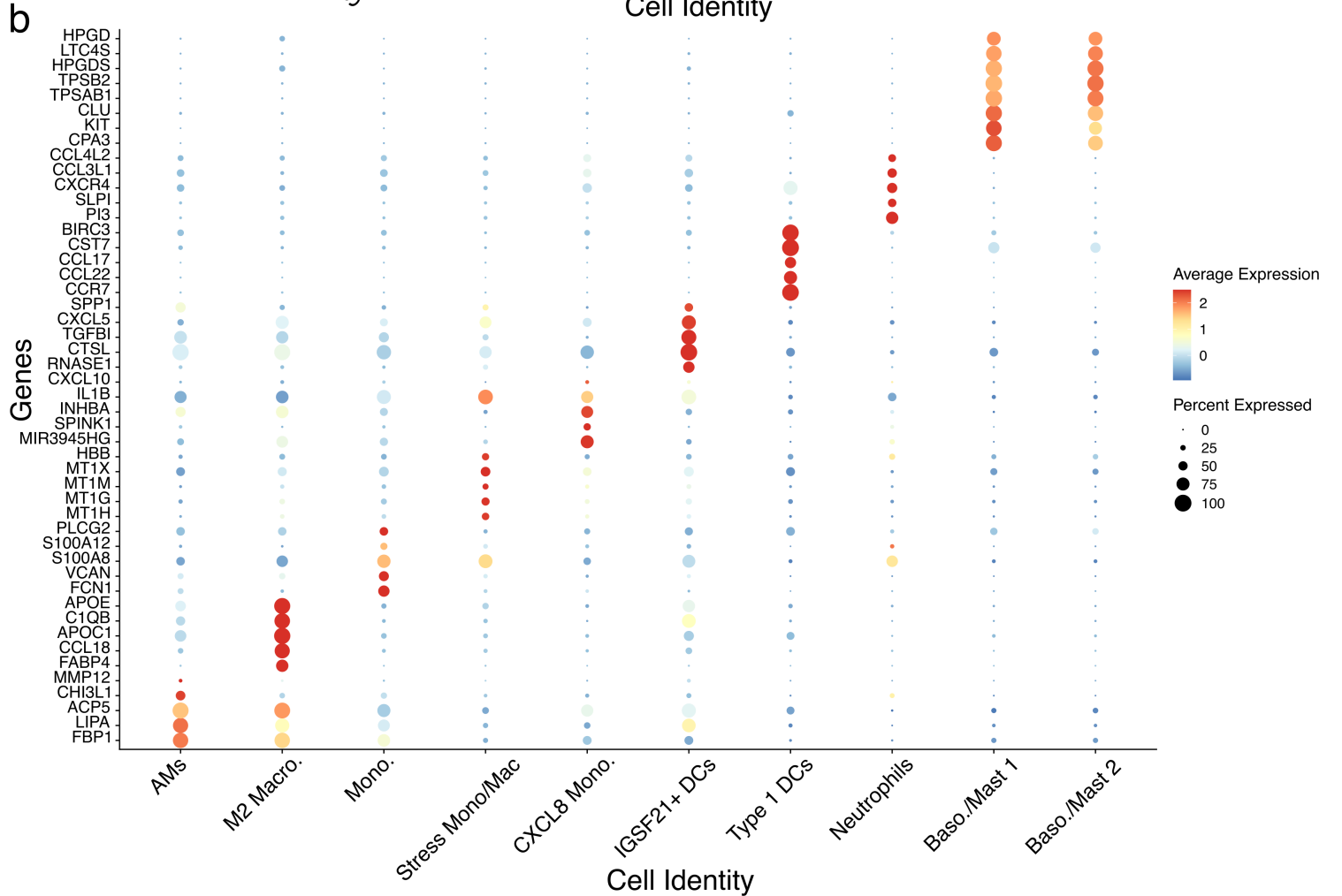
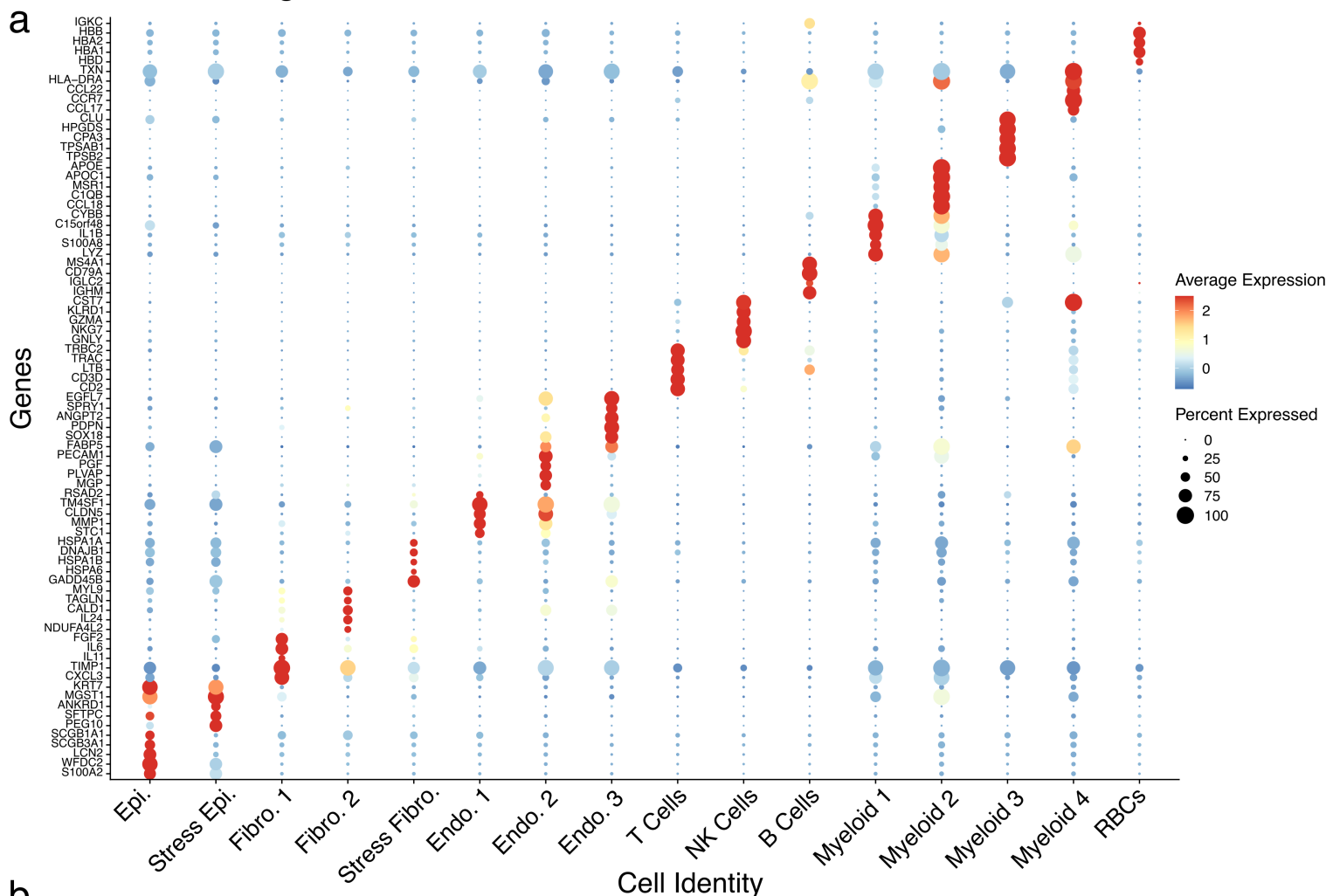


EpCAM dsRNA DAPI

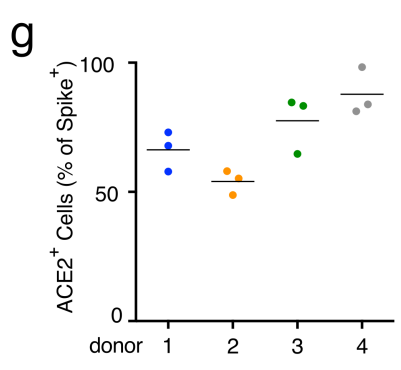
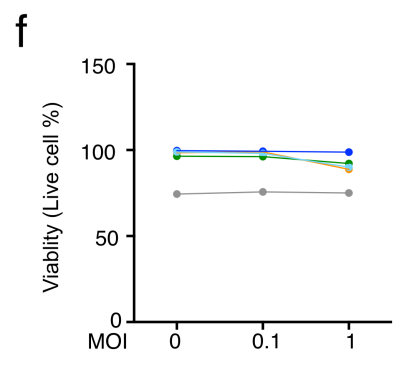
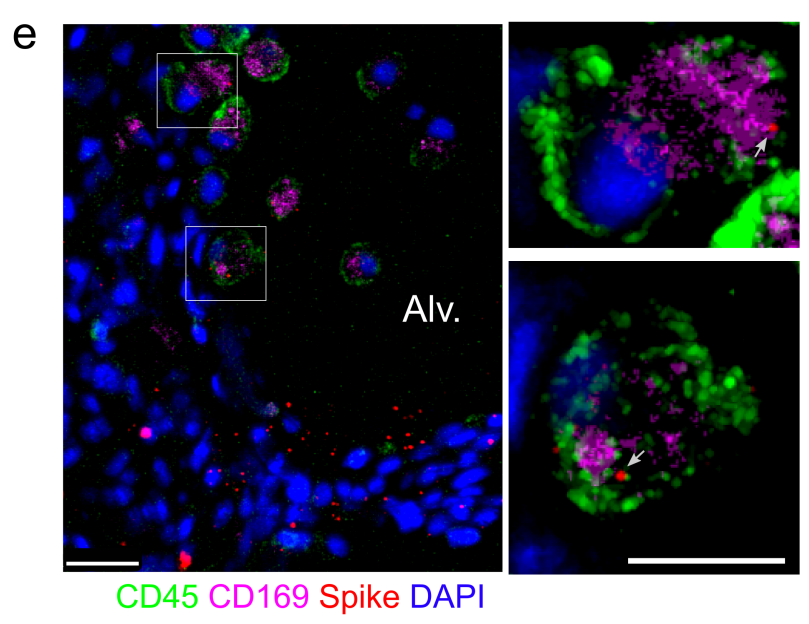
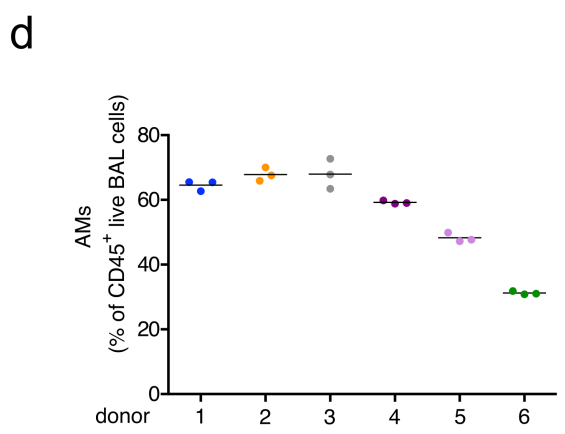
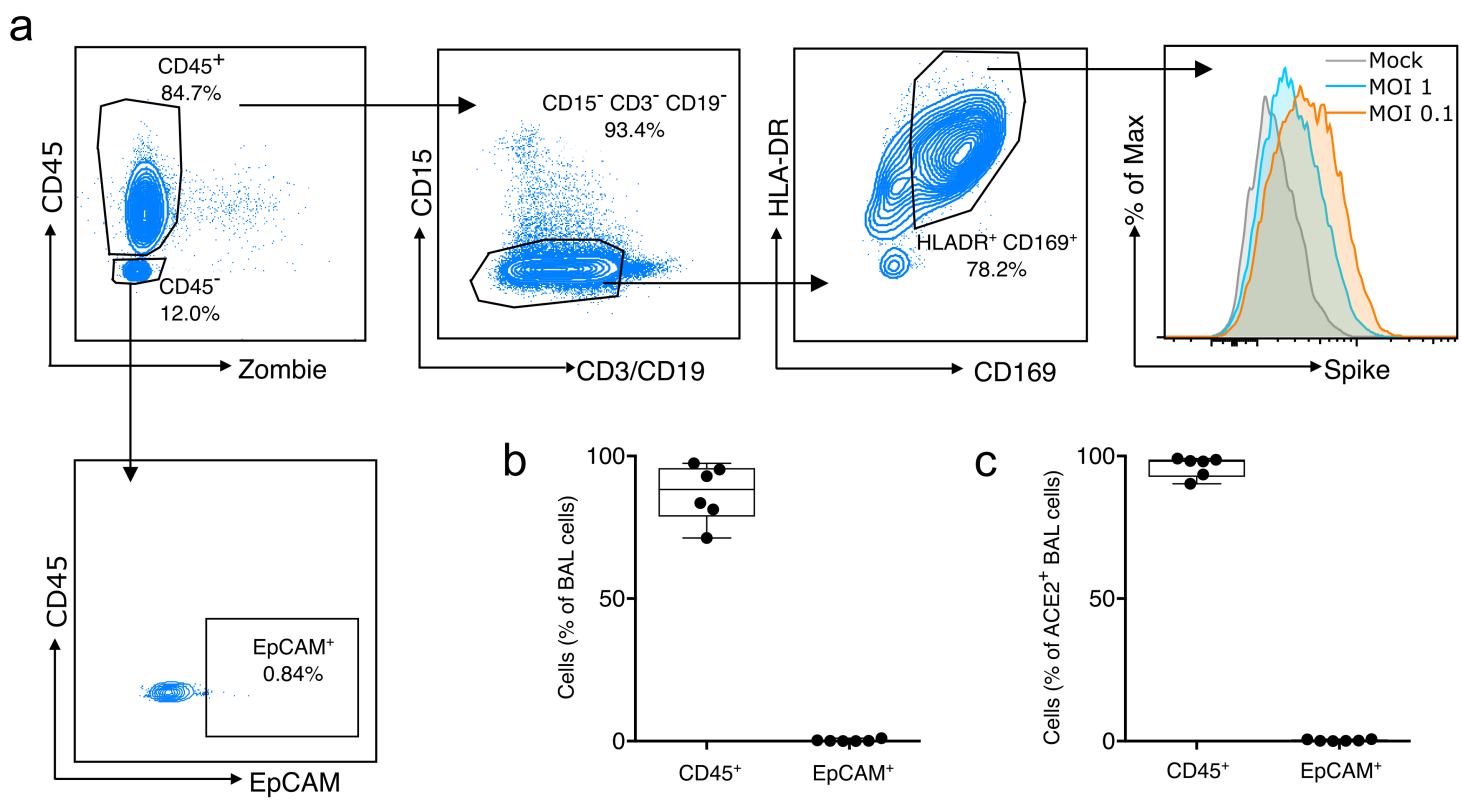


CD45 dsRNA Autofluor DAPI

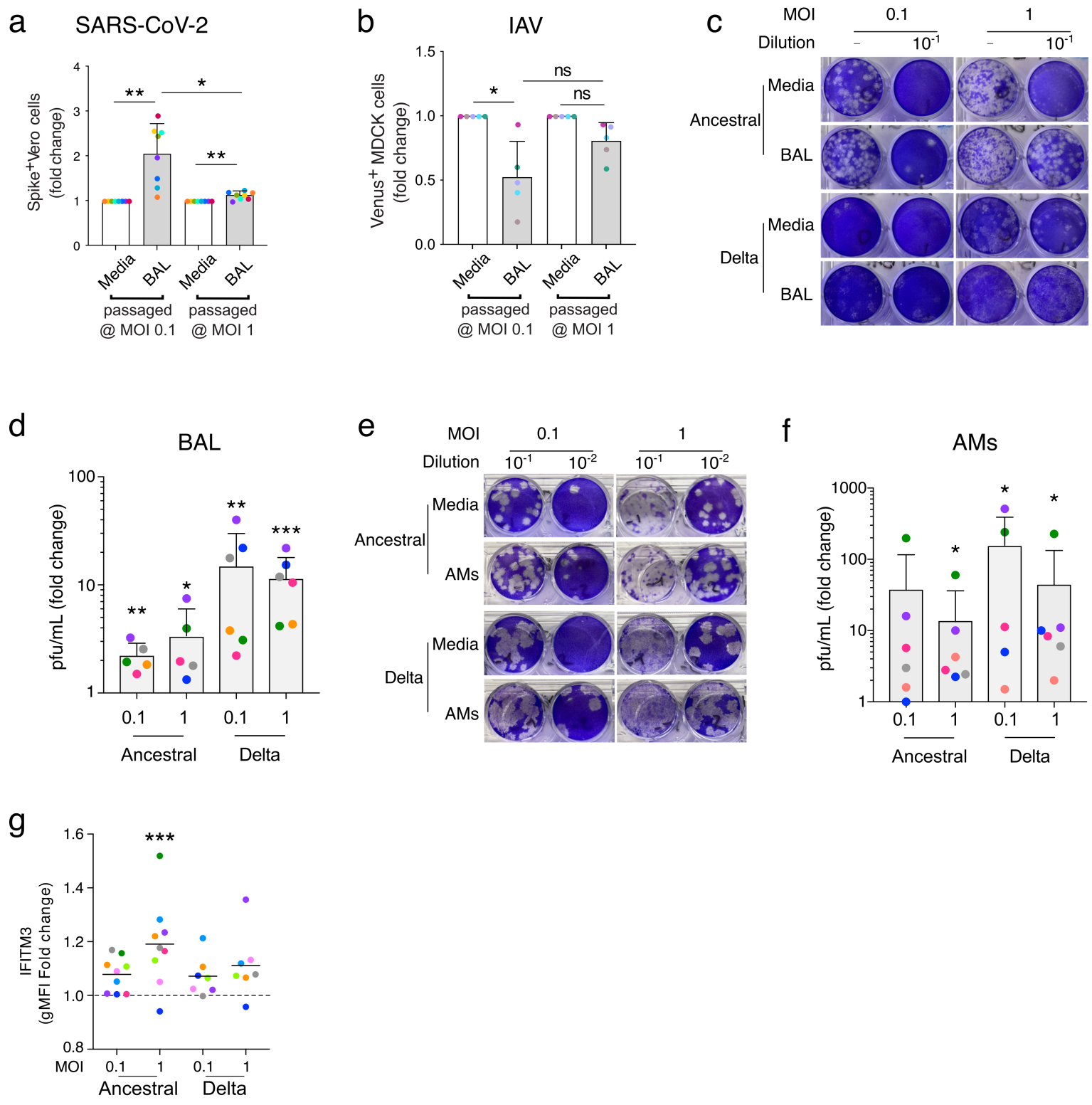
Extended Data Figure 3



Extended Data Figure 4



Extended Data Figure 5



Extended Data Figure 6

